Evaluation of Precoder Designs Using Measured MIMO Channels

ALI ALENEZI

KTH Electrical Engineering

Master's Degree Project
Stockholm, Sweden

XR–EE–SB 2011:008

KTH

Evaluation of Precoder Designs Using Measured MIMO Channels

Ali Alenezi

March 21, 2011

Abstract:

MIMO transceiver designs rely mainly on the knowledge of channel state information (CSI) at the transmitter and receiver sides of a communication link. In most practical scenarios due to the fast fading channels, the transmitter side can only have statistical (or long-term) information about the channel. This thesis investigates and compares five MIMO transceiver designs over a measured 8x4 MIMO channel obtained from ERICSSON in terms of Bit-Error-Rate. Three of the algorithms use statistical channel information (CSI) at the transmitter side and instantaneous channel information at the receiver side, one of the algorithms uses instantaneous channel information at both the transmitter and receiver sides, and one algorithm uses no channel information at the transmitter and instantaneous channel information at the receiver side. The main target of this study is a recently long-term precoder design proposed in [1] which previously has showed good performance compared to other long-term precoder designs on a simulated channel. In the evaluation of the precoder designs on the measured MIMO channel, the precoder in [1] outperformed others long-term precoders and performed near to performance the short-term precoder in [5] on the slow and line-of-sight (LOS) channels. On the fast channels the long-term precoder in [1] works better than other long-term precoders but relatively far from the performance of the short-term precoder.

Acknowledgements

This work would not have been possible without the help, guidance and patience of my two supervisors, Associate Professor Mats Bengtsson and Mr. Simon Järmyr. I would like to thank them for the opportunity to conduct my Master thesis under their supervision.

I would like to thank Omar Aldayel for his advice. I would also like to thank Fadi Al Naji for his help in revising the thesis. I would like to extend my gratitude to my colleagues at the Master thesis room; I will never forget the enjoyable time that we have spent together and the social environment there. I dedicate this thesis to my parents, brothers, and sisters for supporting me during my studies.

Table Of Contents

List of Tables

List of Figures

Notation

In the following we will mention the notations that are used throughout this master thesis. Uppercase boldface letters, i.e. $\boldsymbol{A}$, and lowercase boldface letters i.e. $\boldsymbol{a}$ denote the matrices and the vectors respectively. A submatrix consists of the first i columns of matrix $\boldsymbol{A}$ as denoted by $\boldsymbol{A}_i$, and $\boldsymbol{a}_i$ is denoted the ith column of matrix $\boldsymbol{A}$. The operators $(.)^H$ and $\otimes$ are Hermitian transpose and the Kronecker product respectively, and the operator $(.)^{1/2}$ defines the Cholesky factorization. The operator $Tr(\boldsymbol{A})$ is the trace of the matrix $\boldsymbol{A}$ and $diag[\boldsymbol{a}]$ is the diagonal matrix with a vector $\boldsymbol{a}$ having the diagonal elements.

H	Channel Matrix
$\boldsymbol{R}_{Tx}$	Correlation Transmit Matrix
$\boldsymbol{R}_{Rx}$	Correlation Receiver Matrix
P	Precoder Matrix
W	FeedForward Equalizer
B	Feedback Equalizer
N_{Tx}	Number of Transmit Antennas
N_{Rx}	Number of Receiver Antennas
N_L	Number of Transmitted Symbols

Acronyms

MIMO	Multiple-Input Multiple-Output
CSI	Channel State Information
I-CSI	Instantaneous- Channel State Information
CSIR	Channel State Information at the Receiver side
CSIT	Channel State Information at the Transmitter side
DFE	Decision Feedback Equalizer
MMSE	Minimum Mean-Square Error
MSE	Mean-Square Error
LT DFE	Long-Term Decision Feedback Equalizer
LT LIN	Long-Term LINear receiver
VBLAST	Vertical Bell Laboratories Layered Space-Time
ST DFE	Short-Term Decision Feedback Equalizer
CMD	Correlation Matrix Distance
LOS	Line-Of-Sight
NLOS	Non-Line-Of-Sight
GTD	General Triangular Decomposition
SVD	Singular Value Decomposition
SNR	Signal-to-Noise Ratio
SINR	Signal-to-Interference plus Noise Ratio
BER	Bit-Error-Rate
Min	Minimum
Max	Maximum
Mod	Modulation
Demod	Demodulation
Ch-12	Channel number 12

1 Introduction

A multiple-input multiple-output (MIMO) system uses multiple antennas at both the transmitter and the receiver of the communication link to increase the data rate and the reliability of the communication system. MIMO systems exploit the multiple antennas to form multiple sub-channels to improve a communications system in terms of spectral efficiency and link reliability. Mathematically, a MIMO channel is represented by a channel matrix which provides full information about the nature of a channel. MIMO systems became a significant research field as a result of the high cost of frequency spectrum in commercial wireless systems.

The design of a MIMO transceiver is equivalent to finding the parameters of the equalizer at the receiver and the parameters of the precoder at the transmitter that give an optimized performance under determined constraints, where the channel state information (CSI) is given. To estimate the CSI, the transmitter sends a training sequence or a pilot signal to the receiver side, which is already known to the receiver, to estimate the CSI, and then the receiver transfer the estimated CSI over the feedback channel to the transmitter. The MIMO transceiver based on perfect CSI has been designed optimally in [2].

In practical communication systems, the CSI is far from perfect, for example due to estimation error, quantization error delays that makes the estimates outdated. The imperfection of the CSI at the receiver (CSIR) can be negligible in many cases, while the CSI at the transmitter (CSIT) is far from being perfect in many realistic situations. Many studies have considered the design of MIMO transceivers based on perfect CSIR and imperfect CSIT [1, 3, 4]. The design of imperfect CSIT and perfect CSIR communication systems reduces to a precoder design at the transmitter since the receiver has been optimally designed regardless of the precoder value.

1.1 Objective

The objective of this thesis is to investigate and compare the performance of five precoder designs on measured channel data and evaluate them in terms of Bit-Error-Rate (BER). Three of the considered precoder designs assumed that the imperfect CSIT is available, and all of the precoder designs considered here assume the receiver has full access to the CSI; hence, the receiver always has an optimal design. In order to learn about the loss in the performance of imperfect CSIT precoder designs compared to the perfect CSIT design, we consider the perfect CSIT optimal precoder design [2]. We also consider the VBLAST design evaluation where CSIT is not used, in order to see the improvements in imperfect CSIT precoder designs. All the designs are evaluated over measurements of 8x4 MIMO channels which are obtained from ERICSSON.

Usually, the proposed MIMO transceiver designs are evaluated over simulated channels which are generated according to specific channel conditions. The objective of this

project is to evaluate five MIMO transceiver designs on a measured MIMO channel. In this project we evaluate three long-term CSI precoders [1, 3, 4], one short-term CSI precoder [2], and one with no CSIT precoder [5]. The main focus in this thesis is to evaluate the long-term adaptive pre-coding algorithm proposed in [1], which has shown better performance compared to other long-term precoder methods [3,4].

1.2 Motivation

The main motivation for this thesis comes from recent long-term precoder that was proposed in [1]. The precoder showed good performance compared to other long term precoders designs [3, 4] and approached the performance of the perfect CSIT optimal precoder design [2]. Another main objective is to evaluate the different kind of precoders to determine their performances over a real channel.

1.3 MIMO Channel Measurements

It should be mentioned that the measured channel data for an 8x4 MIMO channel which we used in the evaluation in this thesis was obtained from ERICSSON. The data was recorded during a drive test using LTE testbeds. The drive test took place in Kista Stockholm, where the transmitter was fixed on the top of a building, and the receiver was mounted on a car roof. Figure 1.1 shows the route taken by the mobile-station (MS) during the drive test.

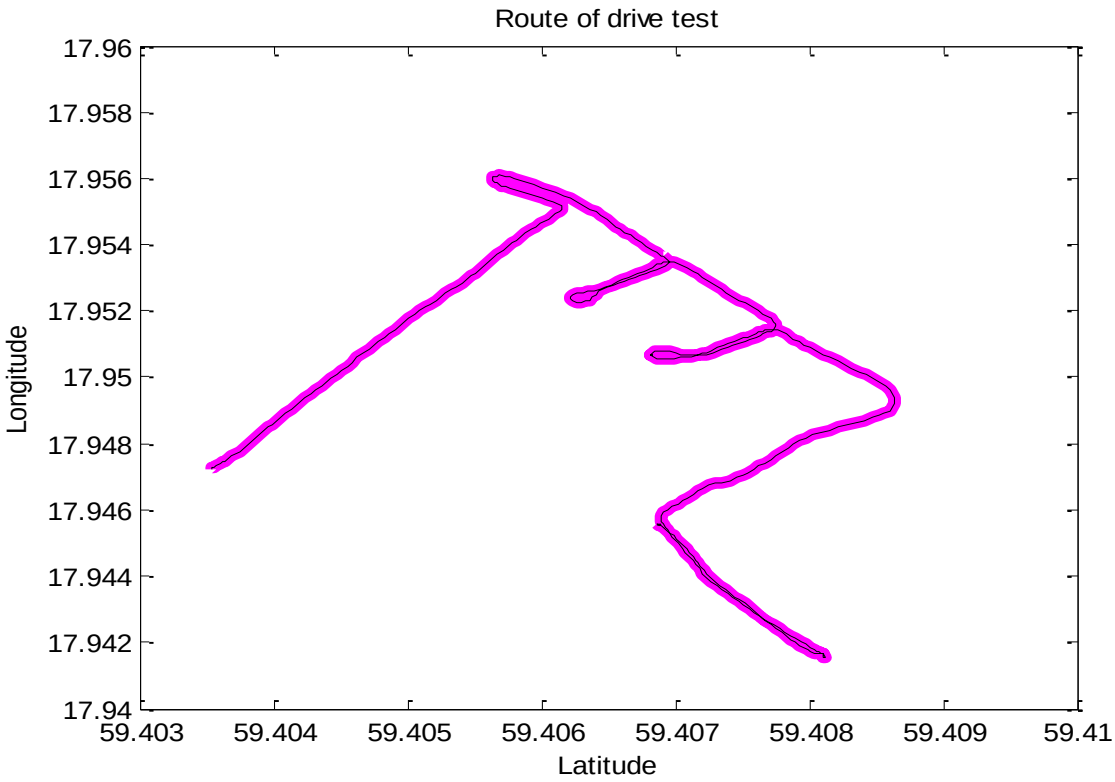

Figure 1.1: GPS Data of a Drive Test by ERICSSON

1.3.1 Measurement Process

The transmitter that contained four cross-polarized antennas was fixed in a line shape on top of a building in Kista. The transmitters were transmitting a training sequence over a bandwidth of 20 MHz, at 2.6 GHz carrier frequency. The receiver that contained four antennas was fixed on a car roof and collected the training sequence and estimated the channel every 5.333 ms with respect to the time and the frequency. Figure 1.2 shows the speed of the MS during the test drive, where the data have been recorded at different car speeds. Various parameters related to the derive test is illustrated in Table 1.1.

Carrier Frequency f_c	2.6 GHz
Wavelength	0.1154 m
Bandwidth	20 MHz
Drive Time	8 min
Average Receiver Speed	18 Km/h
Max Receiver Speed	39 Km/h
Min Receiver Speed	0 Km/h
Samples in Time	87938
Samples in frequency	162
1 Time sample	$\frac{16}{3}$ ms
1 Frequency sample	120 KHz
Drive Test Location	Kista, Stockholm.

Table 1.1: Drive Test Data Details.

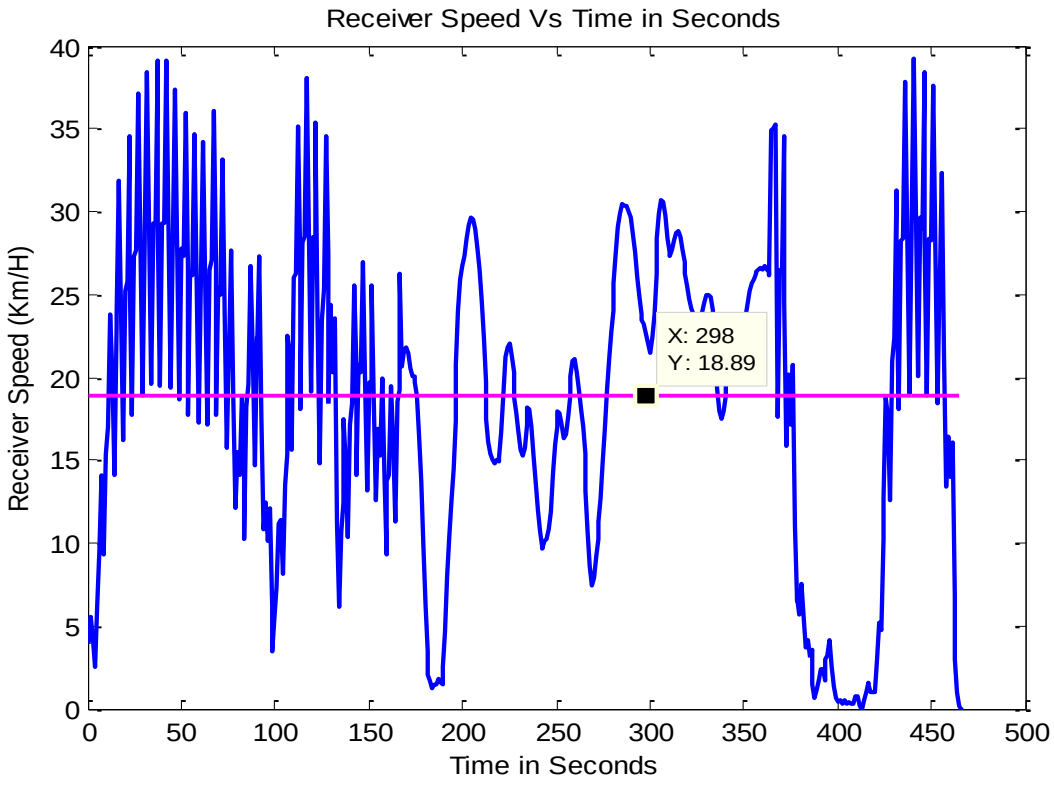

Figure 1.2: GPS speed data of a Drive Test by ERICSSON.

1.3.2 Channel Types

In wireless communications systems, the user-terminal is free to move. As a result, the channel is constantly being changed depending on the location of the transmitter with respect to the receiver and the surrounding environment. To evaluate the considered precoder designs based on the measured channel, we have divided the channel behavior into three channel types, (i) Non-Line-Of-Sight (NLOS) Slow-Fading Channel, (ii) NLOS Fast-Fading Channel, and (iii) Line-Of-Sight (LOS) Channel. These distinctions have been made based on the channel characteristics. The spectrograms of these channels are shown below.

1.3.2.1 Non-Line-of-Sight (NLOS) Slow-Fading Channel

The Slow Fading channel arises from slow changes of the channel characteristics, where the amplitude and the phase of the channel changes slightly relative to time, and can be considered stationary for a period of time. Figure 1.3 shows the spectrogram of the Slow Fading channel; it can be noted from the spectrogram that the amplitude of the channel is barely changing over time.

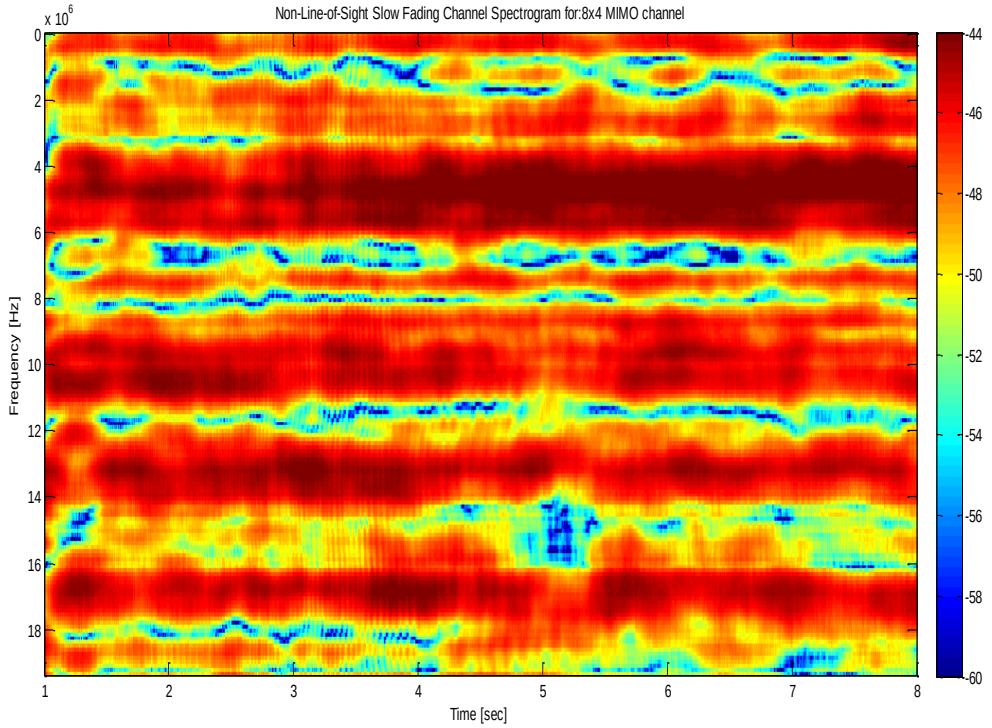

Figure 1.3: NLOS Slow-Fading Channel spectrogram.

1.3.2.2 Non-Line-of-Sight (NLOS) Fast-Fading Channel

Fast fading arises from the quick changing of the channel characteristic in relation to time and frequency. This usually happens due to the moving of the receiver in non-line of sight positions relative to the transmitter. Figure 1.4 shows the spectrogram of the Fast-Fading channel, where the channel changes randomly and rapidly with respect to the time and the frequency

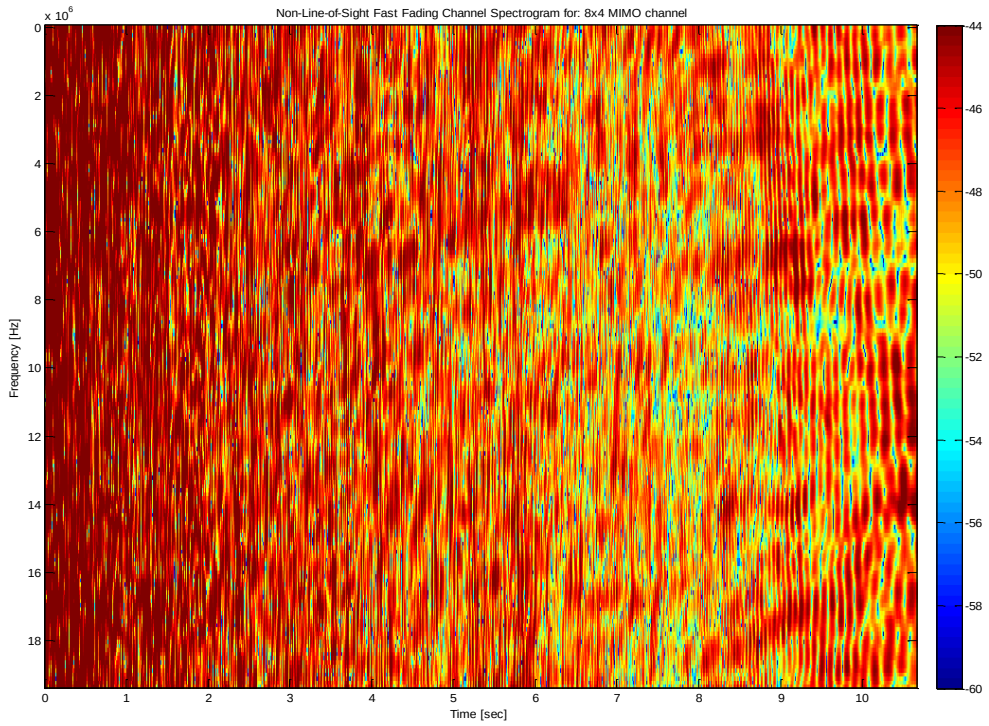

Figure 1.4: NLOS Fast-Fading Channel spectrogram.

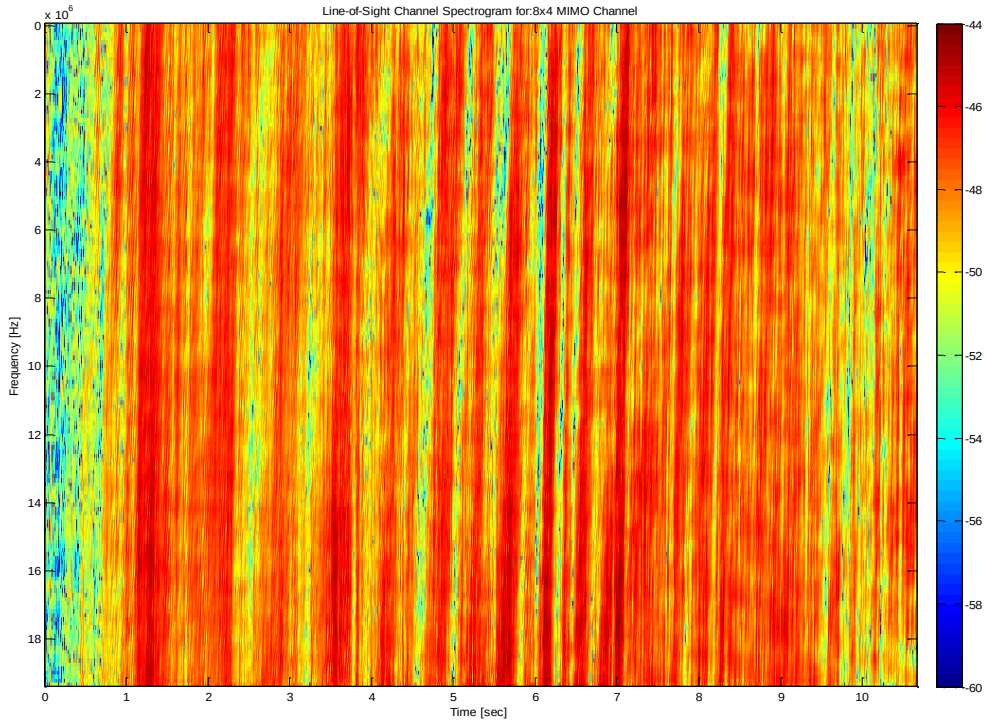

Figure 1.5: Line-Of-Sight Channel spectrogram.

1.3.2.3 Line-of-Sight (LOS) Channel

LOS channel arises when the receiver is moving in line of sight positions relative to the transmitter. As a result, the characteristics of the channel are almost constant in frequency. Figure 1.5 shows the spectrogram of the LOS channel, where the channel amplitude is barely being changed with respect to the frequency.

1.3.3 Antenna Configuration

For the drive test, four x-pol panel transmitter antennas were used, where each x-pol antenna had two dual polarized antenna (one vertical and one horizontal), and they were separated and fixed on top of a tall building as shown in Figure 1.6.a. At the receiver side, four antennas were fixed on the corners of a car's roof as shown in Figure 1.6.b.

a) b)

Figure 1.6: a) Transmitter x-pol antennas fixed on a top of a building. b) Receiver antennas fixed on the corners of car's roof.

Part I

Theory

2. Channel State Information CSI

2.1 Types of CSI

There are two types of CSI; instantaneous CSI and statistical CSI.

a. **Instantaneous CSI** (or short-term CSI): Instantaneous CSI means that the current channel conditions are known.
b. **Statistical CSI** (or long-term CSI): Statistical CSI means that a statistical characterization of the channel is known. This description can include, for instance, (i) the type of fading distribution, (ii) the average channel gain, (iii) the line-of-sight component, and (V) the spatial correlation. As with instantaneous CSI, this information can be used for transmission optimization.

The CSI acquisition is limited by how fast the channel conditions are being changed. In fast fading channels where the channel conditions vary rapidly with the period of one symbol transmission, the receiver can't track the instantaneous changes in the channel conditions. On the other hand, in relatively slightly changing channel conditions, the receiver and transmitter can track the instantaneous CSI with reasonable accuracy and use it for transmission adaptation for some time before becoming outdated.

A precoder design based on the degree of knowledge of CSI can be divided into:

1- Perfect CSIR & perfect CSIT.
2- Perfect CSIR & imperfect CSIT.
3- Imperfect CSIR & Imperfect CSIT.

Perfect CSI means instantaneous CSI (I-CSI) is available, in contrast imperfect CSI means I-CSI is not available; instead the channel distribution information (CDI) is available.

2.2 Statistical Model OF MIMO Channel

Many studies have considered modeling of wireless MIMO channels for the purpose of the system design and evaluation. Here, for the sake of clear presentation, we briefly described the narrowband MIMO channel model that was verified over NLOS indoor MIMO channel measurements in [6,7]. It was observed that the channel covariance matrix could be expressed by the kronecker product of the covariance matrices that are seen in both ends of the communication link as follows:

$$\boldsymbol{R}_H = \boldsymbol{R}_{Tx}{}^{T} \otimes \boldsymbol{R}_{Rx}, \quad (2.1)$$

Where $\boldsymbol{R}_H$ is the channel covariance matrix, $\boldsymbol{R}_{Tx} \in^{N_{Tx} \times N_{Tx}}$ is the transmit correlation matrix and $\boldsymbol{R}_{Rx} \in^{N_{Rx} \times N_{Rx}}$ is the receive correlation matrix. The transmit and receive correlation matrices of the channel matrix $\boldsymbol{H}$ are given by

$$\boldsymbol{R}_{Tx}{}^{T} = \frac{\boldsymbol{E}\left[(\boldsymbol{H}-\widehat{\boldsymbol{H}})^{H}(\boldsymbol{H}-\widehat{\boldsymbol{H}})\right]}{Tr\{\boldsymbol{R}_{Rx}\}}, \qquad (2.2)$$

and

$$\boldsymbol{R}_{Rx} = \frac{\boldsymbol{E}\left[(\boldsymbol{H}-\widehat{\boldsymbol{H}})(\boldsymbol{H}-\widehat{\boldsymbol{H}})^{H}\right]}{Tr\{\boldsymbol{R}_{Tx}\}}, \qquad (2.3)$$

respectively, where $\widehat{\boldsymbol{H}}$ is the mean of the channel matrix. The $Tr\{\boldsymbol{R}_{Tx}\}$ is normalized to be equal to the number of antennas at the transmitter side. Also the channel covariance matrix $\boldsymbol{R}_H$ is given by

$$\boldsymbol{R}_H = \boldsymbol{E}\left[\mathrm{vec}\left((\boldsymbol{H}-\widehat{\boldsymbol{H}})\right)\mathrm{vec}^{\mathrm{H}}\left((\boldsymbol{H}-\widehat{\boldsymbol{H}})\right)\right], \qquad (2.4)$$

where $\mathrm{vec}(\boldsymbol{H})$ is the vector formed by stacking the columns of $\boldsymbol{H}$.

2.3 Channel Matrix Distance (CMD)

To interpret the behavior of a long-term precoder on a certain portion of a MIMO channel, we used the channel matrix distance function to measure the changes in the channel structure with respect to time. The CMD function is based on MIMO correlation matrices $\boldsymbol{R}_{Tx}$ and $\boldsymbol{R}_{Rx}$, and it measures the distance between correlation estimated matrices at different times to characterize how strong the spatial structure of the channel had been changed. For a correlation matrix $\boldsymbol{R}(t)$ that is being changed with time t, the correlation matrix distance between two different times t_1 and t_1 is

$$CDM = 1 - \frac{Tr\{\boldsymbol{R}(t_1)\boldsymbol{R}(t_2)\}}{\|\boldsymbol{R}(t_1)\|_2\|\boldsymbol{R}(t_2)\|_2}, \qquad (2.6)$$

Where $Tr\{\}$ is the trace operator, and $\|.\|_2$ denotes the Frobenius norm. The CMD function was introduced and analyzed using synthetic and measured MIMO data in [8]. The CMD values range from 0 to 1. A 0 value of CMD means the channel structure doesn't change, and 1 means the channel structure changes completely. Based on measured channel data verification, in [8] the threshold where the channel structure is not changed significantly is 0.2.

3 MIMO Transceiver Designs

3.1 Background

The design of a MIMO communication system depends mainly on the degree of knowledge of CSI at both sides of the communication link. Since the channel conditions vary with time, the instantaneous CSI need to be updated in the short term. A popular method for channel estimation at receiver side is so-called training sequence (or pilot sequence), where a known signal is transmitted and then the CSI characteristics are estimated using the priority knowledge of the signal at the receiver side, and the CSI at the transmitter (CSIT) is typically obtained either via a feedback channel from the receiver (this technique requires the channel to be sufficiently slowly varying and it has loss in spectral efficiency), or by exploiting the channel reciprocity (if the uplink and downlink use the same frequency) allowing us to infer the channel from previous receiver measurements.

In practical communication systems the perfect CSI is far from reality due to several imperfections, like (i) estimation error, (ii) quantization error, and (iii) outdated estimation of channels. To get a robust design of a MIMO transceiver through a wireless MIMO channel, the designer should take into account these imperfections in the precoder design problem. In the MIMO systems that work in relatively slow varying channel environments, it is possible to assume perfect CSI at both sides. The design of optimal MIMO transceivers in the presence of perfect CSI at both sides has been studied extensively [2]. In most practical communication systems, when one of the communication terminals is moving (as in GSM network, base-station is fixed, and the user-terminal is freely moving), the channel characteristics are varying rapidly in an unpredictable behavior, which make the tracking of perfect CSI at both sides of the link a difficult task. In wireless communication system, it is practical to assume perfect channel at the receiver side, since the channel estimation sequence is sent in the same block of the transmitted data. However, due to the feed-back problems mentioned above, the transmitter usually can't get instantaneous (or perfect) CSI. As a result, it is more reliable to assume imperfect CSI at the transmitter side in the MIMO transceiver design. There are many MIMO transceiver designs that have considered the uncertainty of the channel at the transmitter side to improve the throughput of the MIMO communication system [1, 3,4].

In the following sections, the theory part of the considered precoders is described. In section 3.2 the general MIMO transceiver structure and signal model of the received signal are introduced. All the precoders considered here are assumed to have perfect CSIR, therefore, the receiver design is always optimum. For the purpose of comparison in the performance loss between the long-term precoders and the short-term precoder (perfect CSIT), the optimal precoder based on perfect CSIT [2] in section 3.3 is described. In section 3.4 the long-term precoder proposed in [1] is described, which is based on the first and second order statistics of the CSI, and is the main precoder of this

thesis. In section 3.5 V-BLAST (no CSIT) [5] is described in order to understand how much gain is added to the MIMO system's performance by the knowledge of long-term CSI. In section 3.6 long-term precoder design based on the second order of the CSI is described [3]. The main difference between the LT precoder proposed in [3] and the LT precoder proposed in [1] is that the precoder in [1] assumed that first and second order statistics of the CSI are available at the transmitter side, in conteast the precoder in [3] assumed only the availability of second order statistic of CSI at the transmitter side. In section 3.7 the long-term precoder with a linear receiver that was proposed in [4] is described. In section 3.8 we mentioned some algorithms that used to generate the precoder matrix in some precoder designs.

3.2 System Model

The baseband signal model corresponding to transmission through a MIMO communication channel of N_{Tx} transmit antenna and N_{Rx} receive antenna is represented by:

$$\boldsymbol{y} = \boldsymbol{H}\boldsymbol{s} + \boldsymbol{n} \qquad (3.1)$$

Where $\boldsymbol{y} \in C^{N_{Rx}}$ is the received vector, $\boldsymbol{H} \in C^{N_{Rx} \times N_{Tx}}$ is the channel matrix, $\boldsymbol{s} \in C^{1 \times N_{Tx}}$ is the transmitted vector, and $\boldsymbol{n} \in C^{N_{Rx} \times 1}$ is a zero-mean circularly symmetric complex Gaussian interference-plus-noise vector with covariance matrix $\boldsymbol{R}_n = \boldsymbol{I}_{N_{Rx}}$.

The structure of a nonlinear MIMO transceiver (linear precoder at transmitter and nonlinear equalizer at receiver) is shown in Figure1. In the beginning we considered all nonlinear MIMO transceiver designs and in the last section we considered the linear MIMO transceiver as a special case (linear precoder at transmitter and linear equalizer at receiver). The transmitted vector from N_{Tx}transmitter antennas can be written as

$$\boldsymbol{s} = \boldsymbol{P}\boldsymbol{x} \qquad (3.2)$$

Where $\boldsymbol{P} \in C^{N_{Tx} \times N_L}$ is the linear precoder matrix, and $\boldsymbol{x} \in C^{N_L}$ is the data vector that contains N_L symbols to be transmitted which were drawn from a set of constellations, where $\boldsymbol{x}$ is assumed to be zero-mean with unit-energy uncorrelated symbols, i.e., $E[\boldsymbol{x}\boldsymbol{x}^H] = \boldsymbol{I}_{N_L}$. We assumed that the number of transmitted symbols $N_L \leq \min(N_{Tx}, N_{Rx})$. The total average transmitted power per transmission (in units of energy) is

$$P_T = E[\|\boldsymbol{s}\|^2] = Tr(\boldsymbol{P}\boldsymbol{P}^H) \quad (3.3)$$

Figure 3.1 shows the general structure of a nonlinear MIMO transceiver, which consists of a linear precoder at transmitter and a DFE at the receiver. The DFE receiver detects the transmitted vector and uses the past detected symbols to eliminate its interference on the late detected symbols; as a result the DFE receiver has a better performance than the linear receiver. If the detection is erroneous, it may cause more errors in the subsequent

detections, which is known as 'error propagation effect'. Based on the assumption that previously detected symbols in the feedback filter are correct, the estimated data vector at the receiver side is:

$$\hat{\boldsymbol{x}} = \boldsymbol{W^H y} - \boldsymbol{Bx} \qquad (\mathbf{3.4})$$

$$= [\boldsymbol{W^H HP} - \boldsymbol{B}]\boldsymbol{x} + \boldsymbol{W^H n}$$

where $\boldsymbol{W} \in C^{N_L \times N_{Rx}}$ is the equalizing filter and $\boldsymbol{B} \in C^{N_L \times N_L}$ is the feedback filter, and where $\boldsymbol{B}$ is an upper triangular matrix under the condition that the equalization process at the receiver start from N_L to 1. In Figure 3.1, $Q[.]$ stands for mapping the estimated signal to the nearest constellation signal.

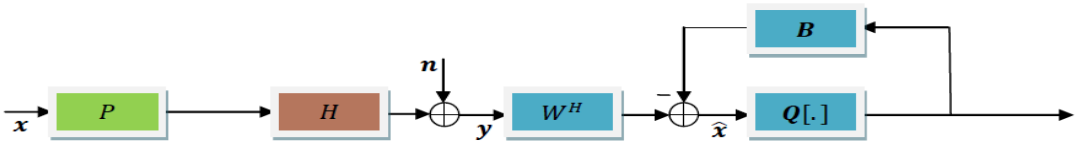

Figure 3.1 General Structure of the MIMO transceiver

One common way to design the nonlinear MIMO transceiver is to formulate the problem in an optimization formula:

$$\min_{\boldsymbol{P,W,B}} \boldsymbol{\mathcal{F}}(\boldsymbol{P,W,B})$$

$$subject\ to\ \ tr(\boldsymbol{P^H P}) \leq P_{max} \qquad (\mathbf{3.5})$$

where $\boldsymbol{\mathcal{F}}$ is the arbitrary cost function, and P_{max} is the maximum expected transmitted power. All considered designs in this thesis considering the mean square error (MSE) matrix of the nonlinear MIMO system as an objective function are to be minimized

$$\boldsymbol{MSE} = E[(\hat{\boldsymbol{x}} - \boldsymbol{x})(\hat{\boldsymbol{x}} - \boldsymbol{x})^H] \qquad (3.6)$$

$$= [\boldsymbol{W}^H \boldsymbol{HP} - (\boldsymbol{B} + \boldsymbol{I})][\boldsymbol{W}^H \boldsymbol{HP} - (\boldsymbol{B} + \boldsymbol{I})]^H + \boldsymbol{W}^H \boldsymbol{R_n W}$$

3.3 Short-Term Nonlinear MIMO Transceiver Design (ST DFE)

The optimal nonlinear MIMO transceiver design is based on the assumption of perfect CSI is available at both the receiver and the transmitter sides. The design of ST DFE has been obtained from [2], that is based on majorization theory. In 3.3.1 and 3.3.2 we provide a brief description of the receiver and transmitter designs in [2].

3.3.1 Optimal Receiver Design

According to the signal model in section 3.2, the estimated substream $\hat{x}_i$ at the receiver side can be written as

$$\hat{x}_i = \boldsymbol{w}_i{}^H \boldsymbol{y} - \sum_{j=i+1}^{N_L} b_{ij} x_j \,, 1 \le i \le N_L \quad (3.7)$$

Denote $\boldsymbol{p_i}$ the ith column of $\boldsymbol{P}$, the performance of substraems measured in terms of the MSE is

$$MSE_i = E[|\hat{x}_i - x_i|^2] \qquad (3.8)$$
$$= |\boldsymbol{w}_i{}^H \boldsymbol{H}\boldsymbol{p}_i - 1|^2 + \sum_{j=i+1}^{N_L} \left|\boldsymbol{w}_i{}^H \boldsymbol{H}\boldsymbol{p}_j - b_{ij}\right|^2 + \sum_{j=1}^{i-1} \left|\boldsymbol{w}_i \boldsymbol{H} p_j\right|^2 + \|\boldsymbol{w}_i\|^2$$

Also, the performance of substreams can be measured in terms of the signal to interference plus noise ratio (SINR) as follows

$$SINR_i \triangleq \frac{desired\ component}{undesired\ component} \qquad (3.9)$$

$$= \frac{|\boldsymbol{w}_i{}^H \boldsymbol{H}\boldsymbol{p}_i - 1|^2}{\sum_{j=i+1}^{N_L} \left|\boldsymbol{w}_i{}^H \boldsymbol{H}\boldsymbol{p}_j - b_{ij}\right|^2 + \sum_{j=1}^{i-1} \left|\boldsymbol{w}_i \boldsymbol{H}\boldsymbol{p}_j\right|^2 + \|\boldsymbol{w}_i\|^2}$$

According to equations (3.8) and (3.9), to minimize the MSEs and maximize the SINRs, the DF coefficients should be

$$b_{ij} = \boldsymbol{w}_i{}^H \boldsymbol{H}\boldsymbol{p}_i, 1 \le i < j \le N_L, \quad (3.10)$$

as a result, the MSEs become

$$MSE_i = |\boldsymbol{w}_i{}^H \boldsymbol{H}\boldsymbol{p}_i - 1|^2 + \sum_{j=1}^{i-1} \left|\boldsymbol{w}_i \boldsymbol{H}\boldsymbol{p}_j\right|^2 + \|\boldsymbol{w}_i\|^2 \quad (3.11)$$

Thus, the optimum feedback matrix $\boldsymbol{B}$ is

$$\boldsymbol{B} = u(\boldsymbol{W}^H \boldsymbol{H}\boldsymbol{P}), \quad (3.12)$$

Where $u(.)$ stands for strictly keeping the upper triangular entries of the matrix while setting the others to zero. Now we need to find the optimum feed-forward filter $\boldsymbol{w}_i$ which minimizes the MSE_i in (3.11). Let $\boldsymbol{G} \triangleq \boldsymbol{H}\boldsymbol{P}$ denote the effective channel matrix. Denoting $\boldsymbol{G}_i \epsilon^{N_R \times i}$ as the submatrix consisting of the first i columns of $\boldsymbol{G}$ and $\boldsymbol{g}_i \epsilon^{N_R \times 1}$ as the ith column of $\boldsymbol{G}$, thus equation (3.11) can be written as

$$MSE_i = \boldsymbol{w}_i{}^H \left(\boldsymbol{G}_i \boldsymbol{G}_i{}^H + I\right) \boldsymbol{w}_i - \boldsymbol{w}_i{}^H \boldsymbol{g}_i - \boldsymbol{g}_i{}^H \boldsymbol{w}_i + 1. \quad (3.13)$$

To minimize MSE_i, equate the derivative of (3.13) with respect to $\boldsymbol{w}_i$ to zero, as a result

$$\left(\boldsymbol{G}_i \boldsymbol{G}_i^{\,H} + I\right)\boldsymbol{w}_i - \boldsymbol{g}_i = 0. \qquad (3.14)$$

Thus, the optimum feed-forward filter for the ith substream is

$$\boldsymbol{w}_i = \left(\boldsymbol{G}_i \boldsymbol{G}_i^{\,H} + I\right)^{-1} \boldsymbol{g}_i, \qquad 1 \le i \le N_L. \qquad (3.15)$$

Substituting $\boldsymbol{W} = \left[\boldsymbol{w}_1, \ldots, \boldsymbol{w}_{N_L}\right]$ in (3.12) yields $\boldsymbol{B}$, both of them represent the optimum filters of DFE. The following result provides a computationally efficient expression for calculating the optimum DFE filters [9, 10].

Lemma 1:

Let the $\boldsymbol{QR}$ decomposition of the argument matrix be

$$\boldsymbol{G}_a = \begin{bmatrix} \boldsymbol{G} \\ \boldsymbol{I}_L \end{bmatrix}_{(N_{Rx}+N_L)\times N_L} = \boldsymbol{QR}. \quad (3.16)$$

Parition $\boldsymbol{Q}$ into

$$\boldsymbol{Q} = \begin{bmatrix} \overline{\boldsymbol{Q}} \\ \underline{\boldsymbol{Q}} \end{bmatrix}, \qquad (3.17)$$

Where $\overline{\boldsymbol{Q}} \epsilon^{N_{Rx}\times N_L}$ and $\underline{\boldsymbol{Q}} \epsilon^{N_L \times N_L}$. Thus, the optimum feed-forward and feedback matrices that minimize the MSEs are

$$\boldsymbol{W} = \overline{\boldsymbol{Q}} \boldsymbol{D_R}^{-1}, \qquad \boldsymbol{B} = \boldsymbol{D_R}^{-1}\boldsymbol{R} - \boldsymbol{I}, \qquad (3.18)$$

Where $\boldsymbol{D_R}$ is a diagonal matrix that has the same diagonal in $\boldsymbol{R}$.Thus, the resulting MSE matrix is diagonal

$$\boldsymbol{E} = \mathbb{E}\left((\hat{\boldsymbol{x}} - \boldsymbol{x})(\hat{\boldsymbol{x}} - \boldsymbol{x})^H\right) = \boldsymbol{D_R}^{-2}. \qquad (3.19)$$

3.3.2 Transmitter Design

Since the receiver side has been optimally designed in the previous section, the problem is reduced to the transmitter side design based on perfect CSI, where the optimization problem reduced to

$$\underset{P}{\text{minimize}}\, f\left(\left\{\boldsymbol{D_R}^{-2}\right\}\right)$$

$$\text{subject to } \begin{pmatrix} \boldsymbol{HP} \\ \boldsymbol{I} \end{pmatrix} = \boldsymbol{QR} \qquad (3.20)$$

$$Tr(\boldsymbol{P}\boldsymbol{P}^H) \le P_o$$

If the cost function $f(.) \in R^{N_L} \to R$ is an increasing function in each argument and $f(\exp(\{\})$ is Schur-convex on R^{N_L}, then, the optimum precoder matrix has the following structure [5]:

$$\boldsymbol{P} = \boldsymbol{V}_H diag\left(\sqrt{p}\right)\boldsymbol{\Omega}^{\mathrm{H}}. \qquad (3.21)$$

and p is the power allocation vector given by the standard water-filling solution

$$p_i = (\mu - \frac{1}{{\Sigma_{ii}}^2})^+, P_{max} = \sum_{i=1}^{K} p_i \qquad (3.22)$$

where $\boldsymbol{V}_H \epsilon^{N_{Tx} \times K}$ comes from the Singular Value Decomposition (SVD) of the channel matrix $\boldsymbol{H}$

$$\boldsymbol{H} = \boldsymbol{U}_{\boldsymbol{H}} \boldsymbol{\Sigma}_{\mathbf{H}} {\boldsymbol{V}_{\boldsymbol{H}}}^{H}. \qquad (3.23)$$

and the semi-unitary matrix $\boldsymbol{\Omega} \epsilon^{N_L \times K}$ is obtained by using the generalized triangular decomposition (GTD)

$$\begin{bmatrix} \boldsymbol{U}_{\boldsymbol{H}} \boldsymbol{\Sigma}_{\mathbf{H}} \mathrm{diag}\left(\sqrt{p}\right) \\ I \end{bmatrix} = \boldsymbol{Q}\boldsymbol{R}{\boldsymbol{P}_J}^{H} \qquad (3.24)$$

such that the matrix $\boldsymbol{R}$ has equal diagonal elements. Table 3.1 gives in a concise way, the optimal design parameters of the nonlinear MIMO transceiver which is based on perfect CSI at both sides of the communication link.

Table 3.1: Short term **N**onlinear MIMO Transceiver design with perfect CSI (ST DFE).

Step	Operation
1	Compute the SVD of $\boldsymbol{H} = \boldsymbol{U}_{\boldsymbol{H}} \boldsymbol{\Sigma}_{\mathbf{H}} {\boldsymbol{V}_{\boldsymbol{H}}}^{H}$.
2	Obtain the optimized power allocations by using waterfilling algorithm $p_i = (\mu - \frac{1}{{\Sigma_{ii}}^2})^+$.
3	Compute the GTD $\boldsymbol{J} = \begin{bmatrix} \boldsymbol{U}_{\boldsymbol{H}} \boldsymbol{\Sigma}_{\mathbf{H}} [\mathrm{diag}\left(\sqrt{p}\right): \mathbf{0}_{K \times (N_L - K)} \\ I \end{bmatrix} = \boldsymbol{Q}\boldsymbol{R}{\boldsymbol{P}_{\boldsymbol{J}}}^{H}$. Where the diagonal elements of R are equal.
4	Obtain the precoder matrix $\boldsymbol{P} = \boldsymbol{V}_H [diag\left(\sqrt{p}\right): \mathbf{0}_{K \times (N_L - K)}] \boldsymbol{P}_J$.
5	Compute the DFE parameters $\boldsymbol{W} = \bar{\boldsymbol{Q}}{\boldsymbol{D}_{\boldsymbol{R}}}^{-1}, \quad and \quad \boldsymbol{B} = {\boldsymbol{D}_{\boldsymbol{R}}}^{-1}\boldsymbol{R} - I.$

3.4 Long-Term Nonlinear MIMO Transceiver Design (LT DFE-1)

The long-term precoder proposed in [1] relies on the first and second-order statistics of the CSI at the transmitter side and on the perfect CSI at the receiver side. The proposed precoder in [1] showed good performance compared to other long-term precoder designs. In section 3.4.1 and 3.4.2 we will describe the transmitter and receiver designs of the long-term precoder obtained from [1].

3.4.1 Receiver Design (DFE)

Since the CSI is perfectly known at the receiver, the optimal design of the receiver side follows exactly the same approach introduced in section 3.3.1 as a function in the channel matrix $\boldsymbol{H}$ and the precoder matrix $\boldsymbol{P}$. Thus, the feed-back matrix $\boldsymbol{B}$ and the feed-forward matrix $\boldsymbol{W}$ are

$$\boldsymbol{B} = u(\boldsymbol{W}^H \boldsymbol{H}\boldsymbol{P}),$$

$$\boldsymbol{w}_i = \left(\boldsymbol{G}_i {\boldsymbol{G}_i}^H + I\right)^{-1} \boldsymbol{g}_i$$

3.4.2 Transmitter Design

Since the receiver parameters, feed-back matrix B and feed-forward matrix W concentrated out from the optimization problem, the optimization problem has been reduced to an optimization of the cost function in (3.20) under the assumption that long-term CSI is only available at transmitter side.

The MSEs are identified by the diagonal elements of the $\boldsymbol{MSE}$ matrix

$$\boldsymbol{E} = \mathbb{E}\left((\hat{\boldsymbol{x}} - \boldsymbol{x})(\hat{\boldsymbol{x}} - \boldsymbol{x})^H\right)$$

$$= [\boldsymbol{W}^H \boldsymbol{H}\boldsymbol{P} - (\boldsymbol{B} + \boldsymbol{I})][\boldsymbol{W}^H \boldsymbol{H}\boldsymbol{P} - (\boldsymbol{B} + \boldsymbol{I})]^H + \boldsymbol{W}^H \boldsymbol{R}_n \boldsymbol{W}. \quad (\boldsymbol{3}.25)$$

Reformulated MSEs and substitute the $\boldsymbol{W}$ and $\boldsymbol{B}$ as functions in the channel matrix $\boldsymbol{H}$ and precoder matrix $\boldsymbol{P}$

$$\boldsymbol{MSE}_i = \boldsymbol{E}_{ii} = 1 - {\boldsymbol{p}_i}^H \boldsymbol{H}^H (\boldsymbol{H}\boldsymbol{P}_i {\boldsymbol{P}_i}^H \boldsymbol{H}^H + \boldsymbol{R}_n)^{-1} \boldsymbol{H}\boldsymbol{p}_i. \quad (3.26)$$

By using the matrix-inversion lemma

$$\boldsymbol{E}_{ii} = \left[(\boldsymbol{I} + {\boldsymbol{p}_i}^H \boldsymbol{H}^H {\boldsymbol{R}_n}^{-1} \boldsymbol{H}\boldsymbol{P}_i)^{-1}\right]_{ii}. \quad (3.27)$$

Since perfect channel is not available at the transmitter side, equation (3.27) should be a function in the expected channel. In [1] by using matrix convexity of the matrix inverse, the lower bound of the expectation of the MSEs is obtained

$$\mathbb{E}(\boldsymbol{E}_{ii}) = \mathbb{E}\left(\left[(\boldsymbol{I} + {\boldsymbol{p}_i}^H \boldsymbol{H}^H {\boldsymbol{R}_n}^{-1} \boldsymbol{H}\boldsymbol{P}_i)^{-1}\right]_{ii}\right) \geq \left[(\boldsymbol{I} + {\boldsymbol{p}_i}^H \widetilde{\boldsymbol{H}}^H \widetilde{\boldsymbol{H}}\, \boldsymbol{P}_i)^{-1}\right]_{ii} \quad (\boldsymbol{3}.28)$$

Where $\widetilde{\boldsymbol{H}}$ is implicitly given by

$$\widetilde{\boldsymbol{H}}^H \widetilde{\boldsymbol{H}} = \mathbb{E}\left(\boldsymbol{H}^H {\boldsymbol{R}_n}^{-1} \boldsymbol{H}\right)$$

$$= \widehat{\boldsymbol{H}}^H {\boldsymbol{R}_n}^{-1} \widehat{\boldsymbol{H}} + \left(\sum_{k,l=1}^{N_{Rx}} \left[{\boldsymbol{R}_n}^{-1}\right]_{kl} [\boldsymbol{R}_H]_{(l+N_{Rx}[j-1]),(k+N_{Rx}[i-1])}\right)_{ij}. \quad (3.29)$$

In this special case, the channel covariance matrix has a Kronecker structure that has been verified in measured data in [8,9] , $\boldsymbol{R_H} = \boldsymbol{R_{Tx}}^T \otimes \boldsymbol{R_{Rx}}$, equation (3.29) reduces to

$$\widetilde{\boldsymbol{H}}^H \widetilde{\boldsymbol{H}} = \widehat{\boldsymbol{H}}^H \boldsymbol{R_n}^{-1} \widehat{\boldsymbol{H}} + tr\left(\boldsymbol{R_{Rx}} \boldsymbol{R_n}^{-1}\right) \boldsymbol{R_{Tx}}^{-1}. \quad (3.30)$$

Since the expected MSEs in (3.28) have the same form of the MSEs of the perfect TX-CSI in section 3.3.1, the long-term precoder follows the same approach of the solution in section 3.3.2 but with expected channel $\widetilde{\boldsymbol{H}}$ instead of instantaneous $\boldsymbol{H}$. Table 3.2 summarizes the procedure design of the long-term precoder with a DF equalizer.

Table 3.2: Long-term precoder design with DFE receiver design (LT DFE -1).

Step	Operation
1	Compute the SVD of $\widetilde{\boldsymbol{H}} = \boldsymbol{U_H} \boldsymbol{\Sigma_H} \boldsymbol{V_H}^H$.
2	Obtain the power allocation by using the water filling algorithm $p_i = (\mu - \frac{1}{\Sigma_{ii}{}^2})^+$.
3	Calculate the GTD $\boldsymbol{J} = \begin{bmatrix} \boldsymbol{U_H} \boldsymbol{\Sigma_H} [\text{diag}(\sqrt{p}) : \boldsymbol{0}_{K \times (N_L - K)} \\ I \end{bmatrix} = \boldsymbol{Q} \boldsymbol{R} \boldsymbol{P_J}^H$. Where the diagonal elements of R are equal.
4	Obtain precoder $\boldsymbol{P} = \boldsymbol{V}_H \left[diag\left(\sqrt{p}\right) : \boldsymbol{0}_{K \times (N_L - K)} \right] \boldsymbol{P}_J$.
5	Compute the DFE $\boldsymbol{W} = \bar{\boldsymbol{Q}} \boldsymbol{D_R}^{-1}$, and $\boldsymbol{B} = \boldsymbol{D_R}^{-1} \boldsymbol{R} - \boldsymbol{I}$.

3.5 VBLAST

The VBLAST design in [5] is based on perfect CSI at the receiver side and no priority knowledge of the channel at the transmitter side. The simple equal power precoder (distribute the total power equally among the transmitted symbols) is used at the transmitter side.

3.5.1 Receiver Design

Based on perfect CSIR, the optimal DFE has been obtained in [5]. The receiver design follows the same approach in the previous sections (receiver design of the optimal transceiver) where the feed-back filter matrix $\boldsymbol{B}$ and feed-forward filter matrix $\boldsymbol{W}$ have the following formula

$$\boldsymbol{B} = u(\boldsymbol{W}^H \boldsymbol{H} \boldsymbol{P}),$$

$$\boldsymbol{w}_i = \left(\boldsymbol{G}_i \boldsymbol{G}_i{}^H + \boldsymbol{I}\right)^{-1} g_i$$

3.5.2 Transmitter Design

The simple precoder are used at the transmitter side, where their function is to distribute the total power equally among the transmitted symbols

$$p_i = \frac{P_{total}}{N_L} \quad 1 \le i \le N_L. \qquad (3.31)$$

where p_i is the transmitted power for the ith symbol, Table 3.3 presents the design's steps for VBLAST.

Table 3.3: VBLAST Design.

Step	Operation
1	Obtain the equal power allocation $p_i = \frac{P_{total}}{N_L}$.
2	Compute the DFE filters $\boldsymbol{W} = \bar{\boldsymbol{Q}}\boldsymbol{D_R}^{-1}, \quad and \quad \boldsymbol{B} = \boldsymbol{D_R}^{-1}\boldsymbol{R} - \boldsymbol{I}$.

3.6 Long-Term Nonlinear MIMO Transceiver Design (LT DFE-2)

The long-term precoder proposed in [3] also performed well compared to VBLAST over a flat-fading MIMO channel. The precoder design in [3] is based on second-order statistics information of the CSI with the assumption that the receiver side has perfect access to CSI.

3.6.1 Receiver Design

The receiver design in [3] optimized according to minimum mean square error (MMSE) criterion under the assumption of perfect channel state information is available at receiver side. The MSE matrix is

$$\boldsymbol{MSE} = \mathbb{E}[\|\boldsymbol{Wy} - \boldsymbol{Bx}\|^2]. \qquad (3.34)$$

From the standard theory of Wiener linear filtering, and after algebraic manipulations, the feed-forward filter matrix is

$$\boldsymbol{w}_i = \left(\boldsymbol{G}_i \boldsymbol{G}_i^{\,H} + I\right)^{-1} \boldsymbol{g}_i, \qquad (\mathbf{3}.35)$$

and the feed-back matrix is

$$\boldsymbol{B} = u(\boldsymbol{W}^H \boldsymbol{H} \boldsymbol{P}), \qquad (3.36)$$

3.6.2 Transmitter Design

Under the assumption that the long-term CSI (LT-CSI) $\mathbb{E}\left[\widehat{\boldsymbol{H}}^H \widehat{\boldsymbol{H}}\right]$ is the only given information to the transmitter, the precoder $\boldsymbol{P}$ has the following form [3]

$$\boldsymbol{P} = \boldsymbol{U}\boldsymbol{\Phi}. \quad (\mathbf{3}.37)$$

where $\boldsymbol{U}$ is obtained from the eigenvalue decomposition of the LT-CSI

$$\mathbb{E}\left[\widehat{\boldsymbol{H}}^H\widehat{\boldsymbol{H}}\right] = \boldsymbol{U}\boldsymbol{\Lambda}\boldsymbol{U}^H. \quad (3.38)$$

and $\boldsymbol{\Lambda}$ is a diagonal matrix that has eigenvalues of $\mathbb{E}\left[\widehat{\boldsymbol{H}}^H\widehat{\boldsymbol{H}}\right]$ at their diagonal, and $\boldsymbol{\Phi}$ is a diagonal matrix such that

$$|\boldsymbol{\Phi}_{ii}|^2 = \left(\frac{N_L + \sum_{n=1}^{\bar{N}} \lambda_{nn}{}^{-1}}{\sum_{n=1}^{\bar{N}} \lambda_{nn}{}^{-1/2}} \ \lambda_{ii}{}^{-1/2} - \frac{1}{\lambda_{ii}}\right)^+. \quad (\boldsymbol{3}.39)$$

where λ_{nn} is the eigenvalue of the expected channel matrix $\widehat{\boldsymbol{H}}$, $(x)^+ = \max(0, x)$ and $\bar{N} \leq N_L$ is such that $|\boldsymbol{\Phi}_{nn}|^2 \geq 0$ for $n \in [1, N_L]$ and $|\boldsymbol{\Phi}_{nn}|^2 = 0$ for all other n. Table 4 summarizes the operations needed to obtain the transmitter and receiver parameters according to the design proposed in [3].

Table 3.4: Long-term nonlinear MIMO transceiver design (LT DFE-2).

Step	Operation
1	Compute the SVD of $\mathbb{E}\left[\widehat{\boldsymbol{H}}^H\widehat{\boldsymbol{H}}\right] = \boldsymbol{U}\boldsymbol{\Lambda}\boldsymbol{U}^H$.
2	Obtain the power allocation $$\|\boldsymbol{\Phi}_{ii}\|^2 = \left(\frac{N_L + \sum_{n=1}^{\bar{N}} \lambda_{nn}{}^{-1}}{\sum_{n=1}^{\bar{N}} \lambda_{nn}{}^{-1/2}} \ \lambda_{ii}{}^{-1/2} - \frac{1}{\lambda_{ii}}\right)^+.$$
3	Obtain precoder matrix $\boldsymbol{P} = \boldsymbol{U}\boldsymbol{\Phi}$
4	Compute the DFE filters $\boldsymbol{W} = \bar{\boldsymbol{Q}}\boldsymbol{D}_{\boldsymbol{R}}{}^{-1}, \quad and \quad \boldsymbol{B} = \boldsymbol{D}_{\boldsymbol{R}}{}^{-1}\boldsymbol{R} - \boldsymbol{I}.$

3.7 Long-Term Linear MIMO Transceiver Design (LT LIN)

All four linear precoder designs described in the previous sections have been optimized jointly with a DFE (nonlinear) receiver. In this section, the proposed linear precoder in [4] that optimized jointly with MMSE linear receiver based on long-term CSI at the transmitter side and perfect CSI at receiver side is described. The difference between the DFE receiver and the linear receiver is that, the DFE uses the feed-back information to cancel the interference effect of the previous detected symbols as shown in Figure3.1, also in the processing aspect, the linear receiver filter can be applied on the receiver symbols simultaneously, in contrast to the DFE receiver that needs to equalize the received symbols successively. Figure 3.2 shows the structure of the linear MIMO transceiver (linear precoder and linear equalizer).

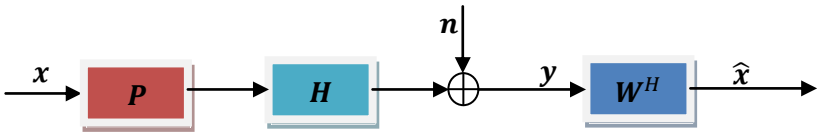

Figure 3.2: Linear MIMO Transceiver.

3.7.1 Receiver Design

As shown in Figure 3.2 the baseband received vector is

$$\boldsymbol{y} = \boldsymbol{HPx} + \boldsymbol{n}. \qquad (\mathbf{3}.40)$$

The constraint on the average transmitted power is

$$Tr(\boldsymbol{PP}^H) \leq P_{max}\,. \qquad (3.41)$$

The linear MIMO transceiver in [4] is optimized based on minimizing the mean square error (MSE) matrix

$$E(\boldsymbol{P}, \boldsymbol{W}) = \mathbb{E}\big((\hat{\boldsymbol{x}} - \boldsymbol{x})(\hat{\boldsymbol{x}} - \boldsymbol{x})^H\big). \qquad (3.42)$$

$$= (\boldsymbol{W}^H\boldsymbol{HP} - \boldsymbol{I})(\boldsymbol{P}^H\boldsymbol{H}^H\boldsymbol{W} - \boldsymbol{I}) + \boldsymbol{W}^H\boldsymbol{R_n}\boldsymbol{W}.$$

where $\boldsymbol{R_n}$ the noise covariance matrix, which has been assumed to be known perfectly at both sides of the link. The linear MMSE receiver $\boldsymbol{W}$ that minimizes the MSE matrix in equation (3.42) is the well-known Wiener filter [11]

$$\boldsymbol{W} = (\boldsymbol{HPP}^H\boldsymbol{H}^H + \boldsymbol{R_n})^{-1}\boldsymbol{HP}. \qquad (\mathbf{3}.43)$$

3.7.2 Transmitter Design

The optimization problem reduced to minimizing the expected MSE with respect to the precoder matrix $\boldsymbol{P}$

$$\mathbb{E}(\boldsymbol{MSE}) = (I + \boldsymbol{P}^H\boldsymbol{\Psi}_{\mathrm{H}}\boldsymbol{P})^{-1}. \quad (3.44)$$

where the equivalent channel covariance matrix is

$$\boldsymbol{\Psi}_{\mathrm{H}} = \widehat{\boldsymbol{H}}\boldsymbol{R}_n{}^{-1}\widehat{\boldsymbol{H}}^H + Tr\big[\boldsymbol{R}_{Rx}\boldsymbol{R}_n{}^{-1}\big]\boldsymbol{R}_{Tx}{}^{T}. \qquad (3.45)$$

where $\widehat{\boldsymbol{H}}$ is the mean of channel matrix, $\boldsymbol{R}_R$ and $\boldsymbol{R}_T$ are the channel covariance matrices seen by the receiver and the transmitter, respectively. The solution for the optimized precoder has the following structure [4]

$$\boldsymbol{P} = \boldsymbol{U}_{\Psi,N_L}\boldsymbol{\Sigma_P}\boldsymbol{V}. \qquad (3.46)$$

where the matrix $\boldsymbol{U}_{\Psi,N_L}$ consists of the N_L eigenvectors of $\boldsymbol{\Psi}_{\mathrm{H}}$ corresponding to the N_L largest eigenvalues in increasing order($\lambda_1 \leq \lambda_1 \leq \ldots \leq \lambda_{N_L}$), $\boldsymbol{\Sigma}_P = \mathrm{diag}[\{\sqrt{p_i}\}]$

contains the power allocation,$\{p_i\}$, in the diagonal, and $\boldsymbol{V}\epsilon^{N_L\times N_L}$ is a unitary matrix such that equation (3.44) has identical diagonal elements. The robust design of linear MIMO transceiver that proposed in [4] is summarized in Table 3.5.

Table 3.5: LT LIN Design.

Step	Operation
1	Compute the SVD of $\boldsymbol{\Psi}_{\mathrm{H}}$ $$\boldsymbol{\Psi}_{\mathrm{H}} = \boldsymbol{U}_{\Psi,N_L}\boldsymbol{\Sigma}_{\boldsymbol{\Psi}_{\mathrm{H}}}{\boldsymbol{U}_{\Psi,N_L}}^{H}$$
2	Obtain the water filling power allocation $$p_i = (\mu - \frac{1}{{\Sigma_{ii}}^2})^{+}.$$
3	Calculate the GTD of $$\boldsymbol{J} = \begin{bmatrix}\boldsymbol{U}_{\boldsymbol{\Psi},N_L}\boldsymbol{\Sigma}_{\boldsymbol{\Psi}_{\mathrm{H}}}[\mathrm{diag}(\sqrt{p}) : \boldsymbol{0}_{K\times(N_L-K)}\\ I\end{bmatrix} = \boldsymbol{QRV}.$$ Where the diagonal elements of R are equal.
4	Obtain precoder $$\boldsymbol{P} = \boldsymbol{U}_{\Psi,N_L}\mathrm{diag}(\sqrt{p})\boldsymbol{V}.$$
5	Compute the MMSE equalizer $$\boldsymbol{W} = (\boldsymbol{HPP}^{H}\boldsymbol{H}^{H} + \boldsymbol{R_n})^{-1}\boldsymbol{HP}.$$

3.8 Precoder

Here we present some important algorithms that we considered to generate the precoder matrix in some MIMO designs.

3.8.1 General Triangular Decomposition (GTD)

Let the structure of the optimized precoder is

$$\boldsymbol{P} = \boldsymbol{V}_H diag(\sqrt{p})\boldsymbol{\Omega}^{\mathrm{H}}. \qquad (4.1)$$

Where $\boldsymbol{\Omega}^{\mathrm{H}}$ is a unitary matrix calculated by using GTD. For the report, we reproduce the theorem of GTD here. For more details about GTD algorithm and implementation refer to [12].

Theorem 4.1: GTD

Assume $\boldsymbol{H}\epsilon^{m\times n}$ to be a matrix with rank K and singular values $\boldsymbol{\sigma}_{\boldsymbol{H},1} \geq \boldsymbol{\sigma}_{\boldsymbol{H},2} \ldots \geq \boldsymbol{\sigma}_{\boldsymbol{H},K} > 0$. There is an upper triangular matrix $\boldsymbol{R}\,\epsilon^{K\times K}$ and semi-unitary matrices $\boldsymbol{Q}$ and $\boldsymbol{P}$ such that

$$\boldsymbol{H} = \boldsymbol{QRP}^{H}$$

If and only if the diagonal elements of $\boldsymbol{R}$ satisfy

$$\prod_{i=1}^{n} \boldsymbol{R}_{ii} \leq \prod_{i=1}^{n} \boldsymbol{\sigma}_{\boldsymbol{H},i} \qquad 1 \leq n \leq K$$

$$\prod_{i=1}^{K} \boldsymbol{R}_{ii} = \prod_{i=1}^{K} \boldsymbol{\sigma}_{\boldsymbol{H},i}$$

Where $\boldsymbol{R}_{ii}$ and $\boldsymbol{\sigma}_{\boldsymbol{H},i}$ values are in non-increasing order [2].

3.8.2 Water Filling

To distribute the total power P_{Total} optimally on the transmit elements, the water filling form is used

$$p_i = (\mu a_i - b_i)^+ \qquad (4.2)$$

Where a_i's and b_i's are some fixed numbers and μ is the waterlevel that has to be calculated such that the power constraint satisfies

$$P_{Total} = \sum_i p_i \qquad (4.3)$$

Part II

Numerical Results

4 Simulation settings

This chapter mainly deals with the simulation settings and assumptions used to generate the numerical results in this thesis. This information is being mentioned here, so that it may be possible for others to reproduce similar results.

4.1 Basic Assumptions

We used MATLAB software to do all simulations in this thesis work. The system model used to simulate the nonlinear MIMO system (linear precoder at transmitter and decision feedback equalization at receiver) is shown in Figure 4.1. The transmission bits are represented by **b** which is independent and identically distributed (I.I.D). We use QPSK modulation to convert $\boldsymbol{b}$ bits into symbols and form a vector of N_L symbols and pass it to precoder block for preprocessing using precoder matrix $\boldsymbol{P} \epsilon^{N_{Tx} \times N_L}$. The output of the precoder block is sent through $N_{Rx} \times N_{Tx}$ $MIMOchannel$ where we assume that zero-mean noise with identity covariance matrix $\boldsymbol{n} = \mathcal{CN}(\boldsymbol{0}, \boldsymbol{R_n} = \boldsymbol{I})$ is added to the channel response vector.

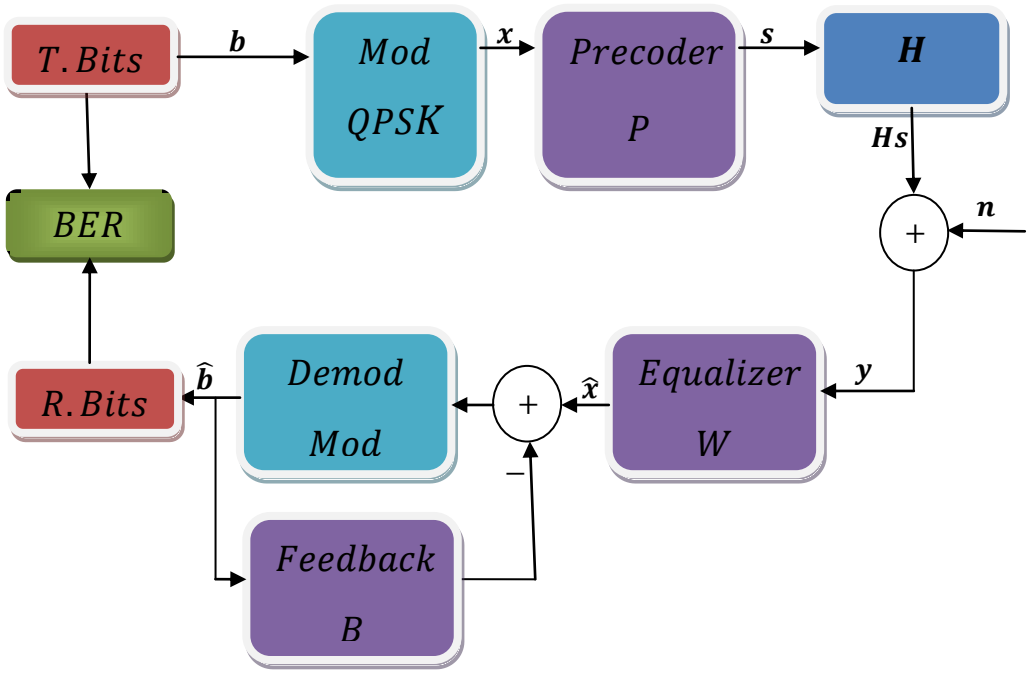

Figure 4.1: General structure of the simulator.

At the receiver side, MMSE filter equalizes each symbol in the received vector ($\boldsymbol{y} = [y_1, \dots, y_{NL}]$) one by one such that it equalizes first the symbol y_{NL}, and passes the result $\hat{x}_{N_L}$ into $Modem/Mod$ to recover the nearest constellation. Then $\hat{x}_{N_L}$is fed back to cancel its interference from the next equalized symbol $\hat{x}_{N_L-1}$ and so on. Finally, the estimated received symbols are converted back into bits and then compared with the transmitted bits to calculate the Bit-Error-Rate (BER) of the system.

4.2 Modulation Scheme

We used Gray coding QPSK modulation in all simulations in this thesis. QPSK uses four points on the constellation diagram, equally spaced around a circle. With four phases, QPSK can encode two bits per symbol with Gray coding mode.

4.3 Channel Normalization and large scale fading effect

In a wireless communication system the transmitted signals arrive to the receiver by multiple paths and due to the constructive and destructive addition of received signals at the receiver side, the resulted received signal is subjected to the problem of amplitude fluctuations with respect to time. Since the measured channel data were recorded when the receiver terminal was moving, it resulted in large scale fading effects on the measurements of the channel. Therefore, we have carefully choose the portions of the channels that don't have large scale fading samples, and then we applied channel normalization on them in order to have fair signal-to-noise ratios (SNR) in simulations. We use the following method to normalize the channel matrices. Consider the received signal model given by:

$$\boldsymbol{y} = \mathbf{H}\boldsymbol{P}\boldsymbol{x} + \boldsymbol{n}, \qquad (4.4)$$

Thus, signal to noise ratio is

$$SNR = \frac{E[\|\mathbf{H}\boldsymbol{P}\boldsymbol{x}\|^2]}{E[\|\boldsymbol{n}\|^2]}, \qquad (4.5)$$

Where $\boldsymbol{n} \in C^{N_{Rx}\times 1}$ is a zero-mean circularly symmetric complex Gaussian vector with covariance matrix $\boldsymbol{R}_n = \boldsymbol{I}_{N_{Rx}}$.

$$E[\|\boldsymbol{n}\|^2] = Tr(\boldsymbol{R}_n) = Tr(I) = N_{Rx}, \qquad (4.6)$$

Where $\boldsymbol{x}$ is assumed to be zero-mean with unit-energy uncorrelated symbols

$$E[\boldsymbol{x}\boldsymbol{x}^H] = \boldsymbol{I}_{N_L} \qquad (4.7)$$

In order to have constant contribution in the resulted SNR at the receiver side, we normalized the channel matrix such that the

$$SNR = Tr(\boldsymbol{P}\boldsymbol{P}^H) = P_{Total}, \qquad (4.8)$$

Hence we can control the SNR of the system from the precoder matrix. Therefore, the channel is normalized in time using the formula shown below.

$$\mathbf{H}_n(n) = \frac{\mathbf{H}(n)\sqrt{N_{Tx}N_{Rx}}}{\sqrt{\frac{1}{N}\sum_{n=1}^{N}\|\mathbf{H}(n)\|^2{}_F}}, \qquad (4.9)$$

4.4 Decision Feedback Equalizer

It is worthwhile noting that, the DF equalizer has error propagation. Therefore the DFE should detect the substream with the smallest error probability first in order to minimize the error propagation toward the substreams detected later.

4.5 System Performance

The performance of the considered precoders is measured in terms of BER for a QPSK constellation (M=4), for measured 8×4 MIMO channel. The BER is evaluated at different SNR levels using Monte Carlo simulations.

4.6 Statistical Channel parameters Estimation

In simulation settings in long-term precoder designs, we use the estimation interval samples N_P to estimate the statistical parameters of the channel, and then we use this statistical parameter to calculate the precoder matrix to use it for the transmitting on the evaluation interval samples N_F in order to make it a causal system. At the receiver side, we use the instantaneous CSI (I-CSI) which updated every $\frac{16}{3}\ ms$. In the perfect CSI MIMO transceiver design, we use the same I-CSI at both sides of the communication link.

5 Results

5.1 General Trends

The main observation of this thesis is the long-term precoder proposed in [1] that showed good performance in terms of numerical simulations compared to other long-term designs. In this section we use a measured MIMO channel obtained from ERICSSON to evaluate the performance of precoder designs considered in this thesis in term of BER. Table 5.1 summarizes the differences between the precoders.

Precoder Name	CSI at the transmitter	CSI at the receiver	Receiver Type
ST DFE	Short-term CSI	Short-term CSI	Nonlinear receiver (DFE)
LT DFE-1	First and second orders statistics of CSI	Short-term CSI	Nonlinear receiver (DFE)
LT DFE-2	Second order statistic of CSI	Short-term CSI	Nonlinear receiver (DFE)
LT LIN	First and second orders statistics of CSI	Short-term CSI	Linear Receiver (MMSE)
VBLAST	No CSI	Short-term CSI	Nonlinear receiver (DFE)

Table 5.1: Precoders Characteristics.

5.2 8x4 MIMO Channel for $N_L = 4$

In this section, five MIMO transceiver designs are evaluated over 8x4 MIMO measured channels. The data rate of the MIMO system is 4 $symbols/channel\ use$. We have picked up different portions from the measured channel which have different characteristics. The highlighted sections in Figure 5.1 represent the considered channel portions and their code number. Based on the spectrograms of the channel portions, we have classified them to certain channel types as shown in the colored sections in Figure 5.1.

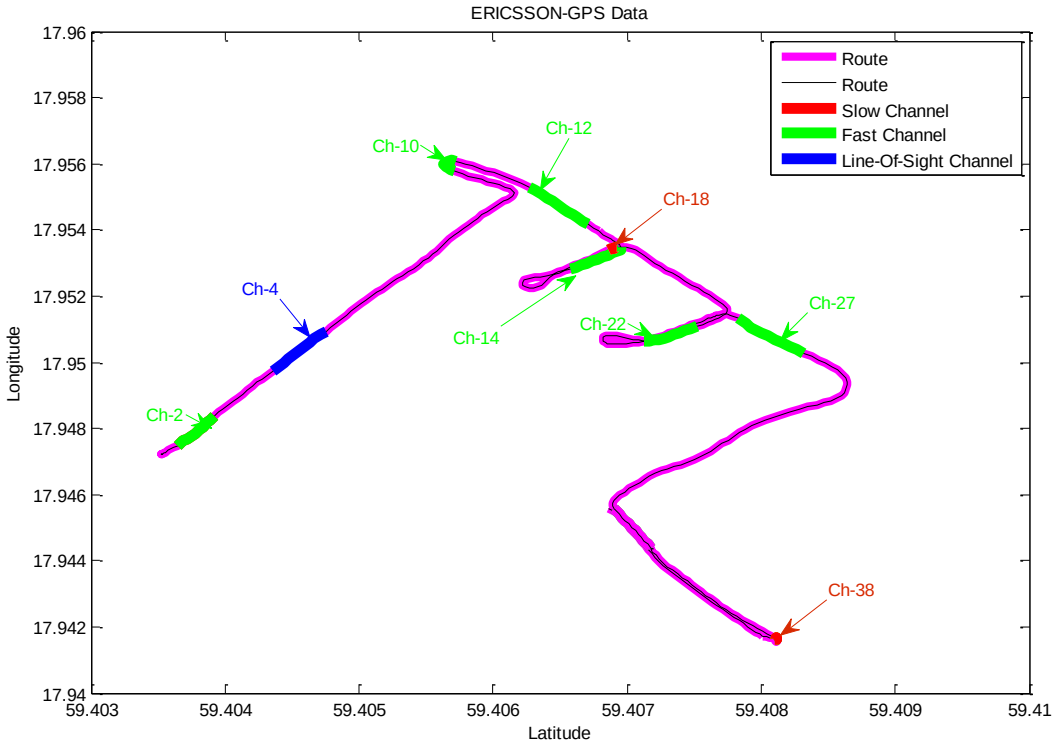

Figure 5.1: Highlight sections refered to the channel portions that considred in the evaluation.

To get information about a channel's charactristics, we have included plots of the spectrogram and eigenvalues variation for each considred channel portion. Also to get information about the changing of the channel structure over time, we plot the correlation matrix distance (CMD) between the estimated correlation matrix

$$\widehat{\boldsymbol{R}}_{Tx} = \frac{1}{N_P}\sum_{n=1}^{N_P} \boldsymbol{R}_{Tx}(n), \qquad (5.1)$$

and the correlation transmit matrices of the evaluation interval $[\boldsymbol{R}_{Tx}(1), \boldsymbol{R}_{Tx}(2), \dots, \boldsymbol{R}_{Tx}(N_F)]$ (or that channel that used to evaluate a precoder performance). To be causal system evaluation, we use N_P past 8×4 MIMO channel samples to estimate the long term precoder parameters, and then we use the estimated precoder to preprocess symbols that are going to transmit over the next N_F channel samples as shown in Figure 5.2

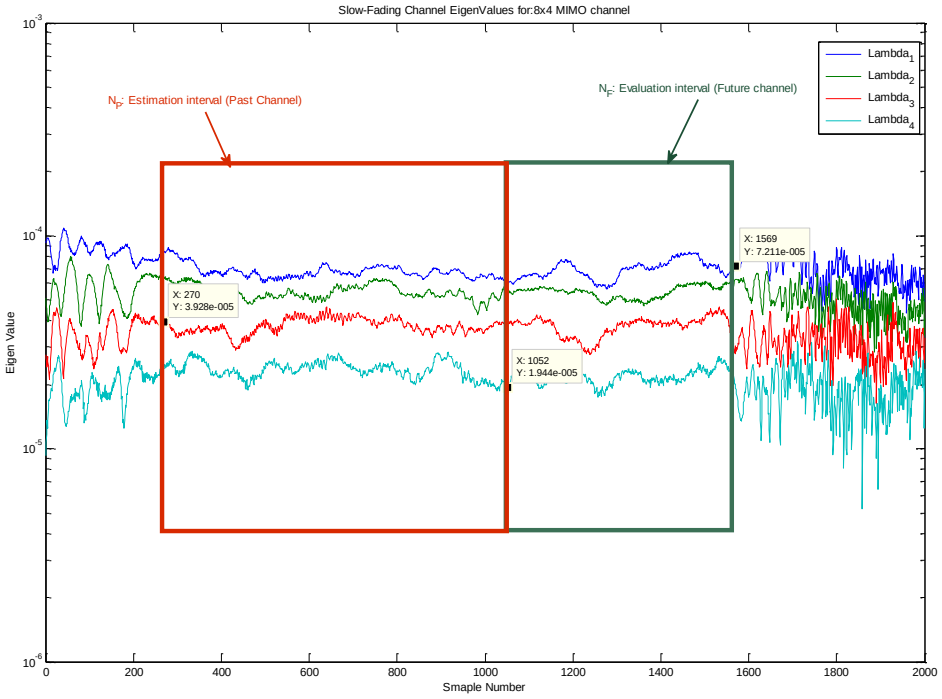

Figure 5.2: The eigen-Values Slow-Fading Channel, where N_F *and* N_P are the evaluation interval (future channel samples) and the estimation interval (past channel samples), respectively.

5.3 Slow-Fading Channel

We have classified the channel Ch-18 and Ch-38 as slow fading channels based on their spectrograms shown in Figure 5.3 (left). Also their eigenvalues that change over time are plotted in Figure 5.3 (right).

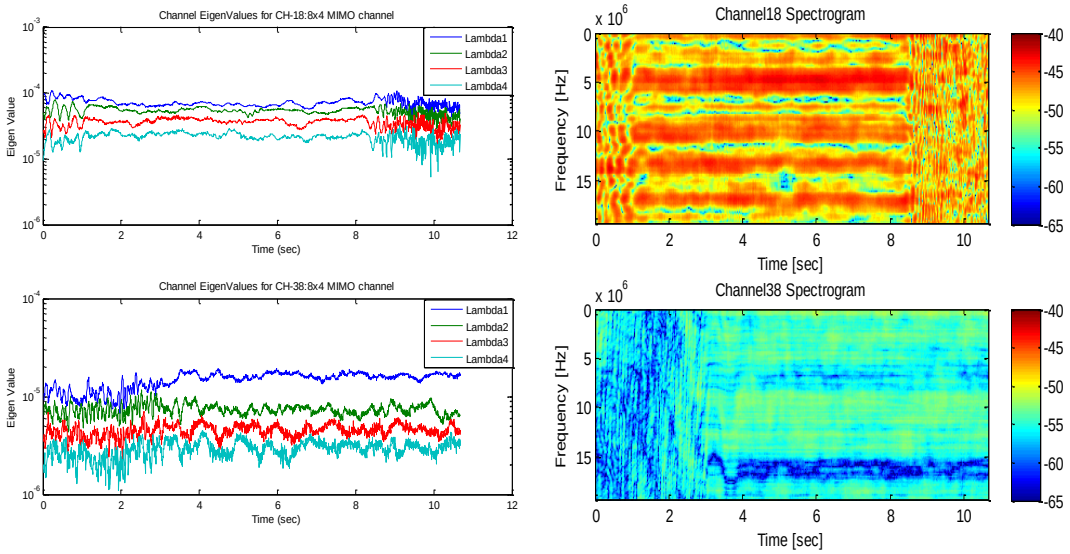

Figure 5.3: Left) Ch-18 and Ch-38 eigenvalues. Right) Ch-18 and Ch-38 Spectrograms.

5.3.1 Slow Fading Ch-18 BER Vs. SNR

Figure 5.4.(Left) shows the performance of the considered precoder designs over the measured channel Ch-18 in term of BER versus SNR. Also the CMD between the expected correlation transmit matrix of the estimation interval and the correlation transmit matrices of the evaluation interval is shown in Figure 5.4.(Right). Table 5.1 presents the values of the evaluation interval N_F and estimation interval N_P expressed in meters, as well as the average speed of the receiver.

Average receiver Speed	*2.51 km/h*
Distance of evaluation interval N_F	0.37 m
Distance of estimation interval N_P	3.33 m

Table 5.2 Channel 18 speed and distance information

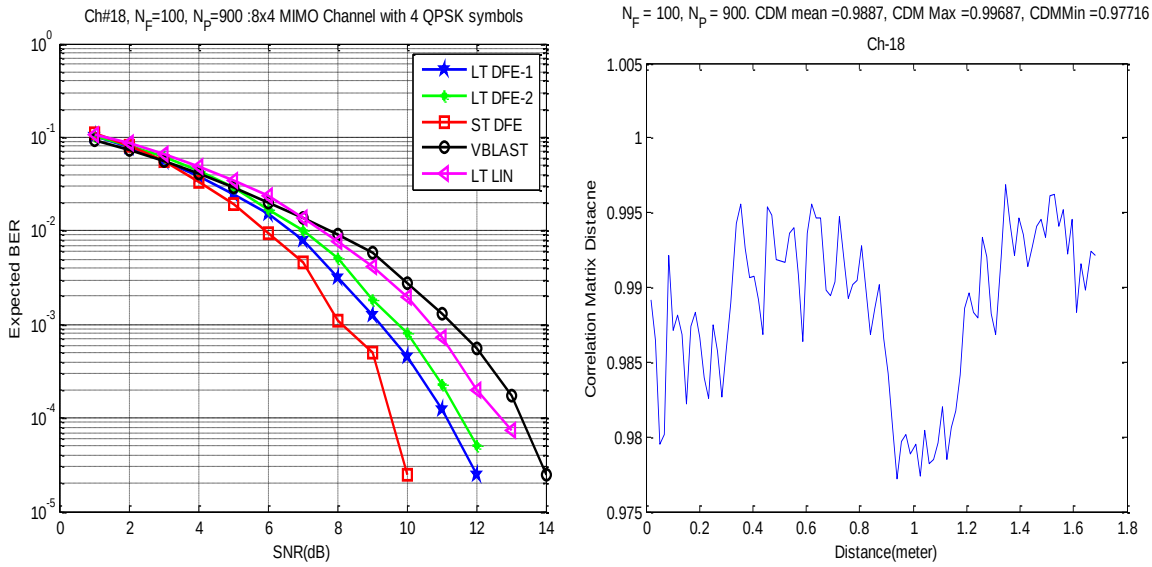

Figure 5.4: Left) Performance of precoder designs over Ch-18 in terms of BER. Right) CMD of Expected $\boldsymbol{R}_{Tx}$ of estimation interval with $\boldsymbol{R}_{Tx}$'s **o**f evaluation interval.

On the NLOS slow channel (Ch-18), the LT DFE-1 precoder performs better than other long-term precoders (LT DFE-1 and LT LIN). Since the LT LIN uses linear equalizer at the receiver side, we always expect LT LIN precoder to be worse than LT DFE-1 precoder at high SNR. All precoder designs outperform the VBLAST design that doesn't use any CSI at the transmitter side. It is clear that the short-term CSI precoder (ST DFE) works better than other precoders as expected. As shown in figure 5.4 (right), the structure of the expected correlation matrix of the estimation interval has week correlation with the correlation matrices of the evaluation interval.

5.3.2 Slow Fading Ch-38 BER Vs. SNR

Average receiver Speed	1.87 km/h
Distance of evaluation interval N_F	0.21 m
Distance of estimation interval N_P	3.95 m

Table 5.3 Channel 38 speed and distance information

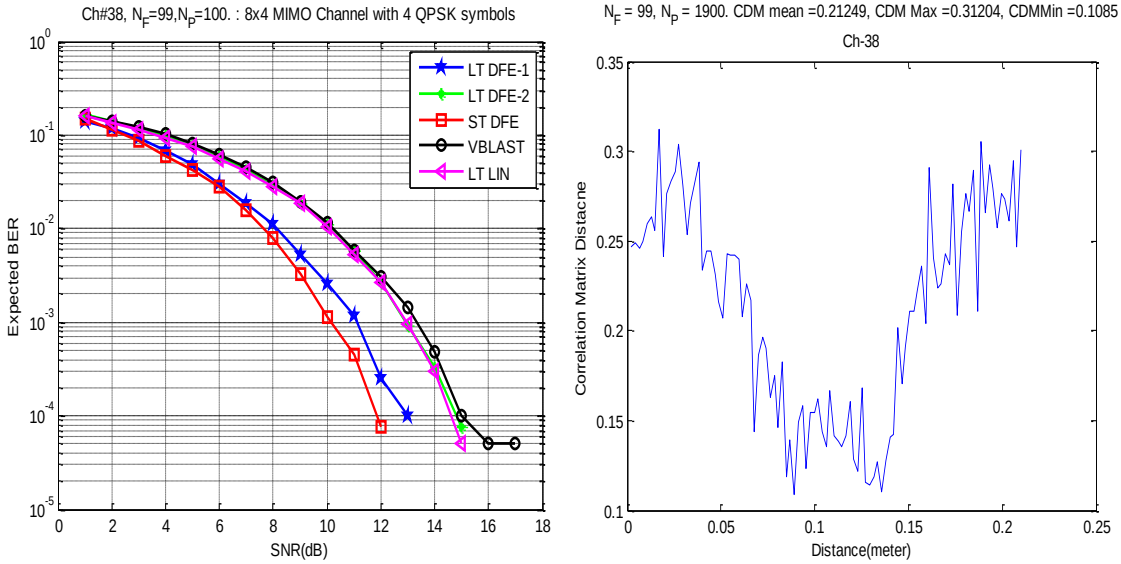

Figure 5.5: Left) Performance of precoder designs over Ch-38 in terms of BER. Right) CMD of Expected $\boldsymbol{R}_{Tx}$ of estimation interval with $\boldsymbol{R}_{Tx}$'s **o**f evaluation interval.

In Figure 5.5 (left) the LT DFE-1 precoder outperforms the other long term precoders and the VBLAST, and approaches the performance of the optimal precoder design (ST DFE). It is clear from Figure 5.5. (right) that the expected correlation transmit matrix of the estimation interval has stronger correlation with the correlation transmit matrices of the evaluation interval compared with Ch-18.

5.4 Line-Of-Sight Channel

Ch-4 is classified as a Line-Of-Sight channel according to their spectrogram that is shown in Fig.5.6. Figure 5.6 also shows the eigenvalues of Ch-4 that vary with time.

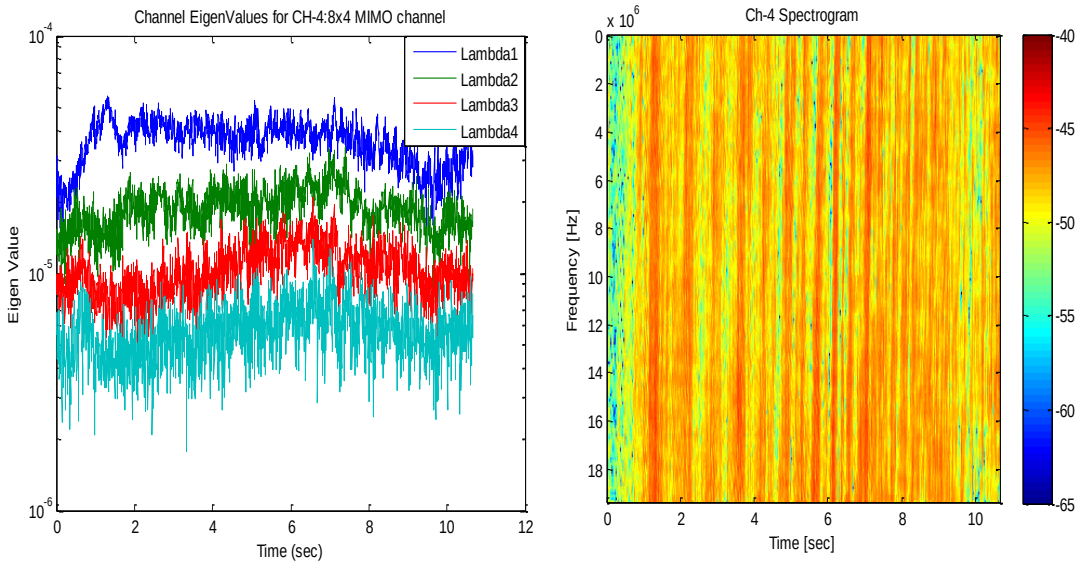

Figure 5.6: Left) Ch-4 eigenvalues. Right) Ch-4 Spectrogram.

5.4.1 Line-Of-Sight Ch-4 BER Vs. SNR

Average receiver Speed	27.5 km/h
Distance of evaluation interval N_F	4 m
Distance of estimation interval N_P	77 m

Table 5.4 Channel 4 speed and distance information

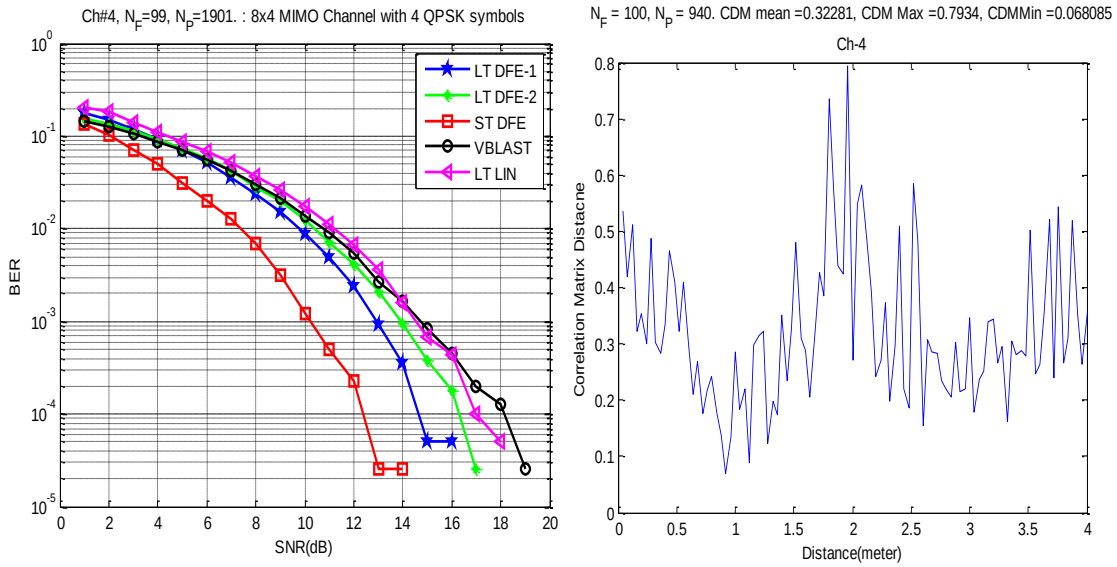

Figure 5.7: Left) Performance of precoder designs over Ch-4 in terms of BER. Right) CMD of Expected $\boldsymbol{R}_{Tx}$ of the estimation channel with $\boldsymbol{R}_{Tx}$'s **o**f evaluation channel.

In Figure 5.7 (left) the LT DFE-1 precoder works better than other long-term precoders and VBLST. Figure 5.7. (right) clearly shows the significant change in the channel structure of the evaluation interval compared with the estimation interval.

5.5 Fast-Fading Channel Ch-2 and Ch-10

The Non-Line-Of-Sight Fading (NLOF) channel is due to fast changing in the channel parameters. Since the fast fading channel is the most common channel in the wireless channels, we considered 6 channel portions in the precoder design evaluations. Ch-2, Ch-10, Ch-12, Ch-22, and Ch-27 are classified as fast-fading channels according to their spectrograms that are shown in Figure 5.8, Figure 5.11 and Figure 5.14.

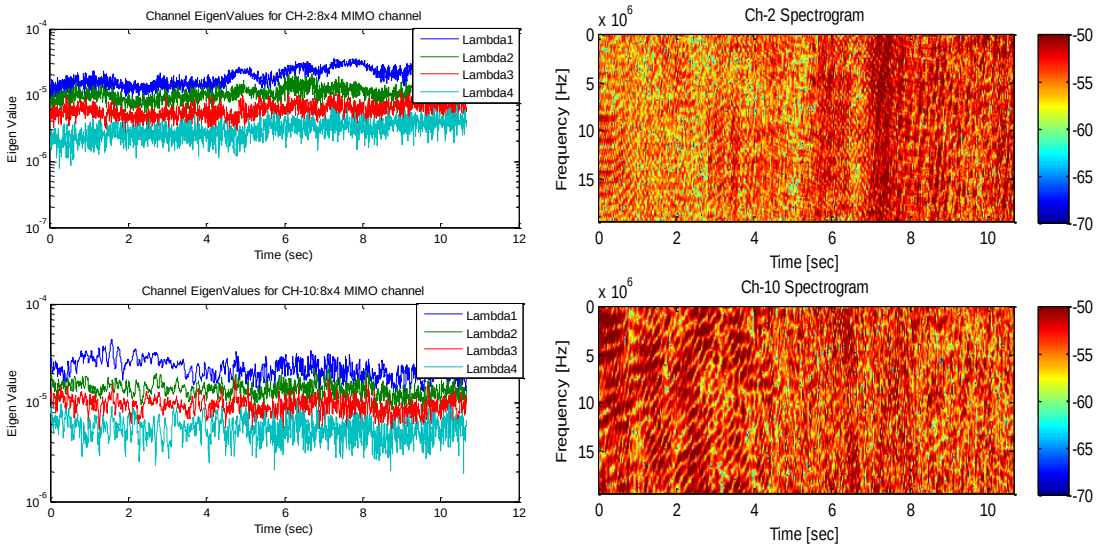

Figure 5.8: Left) Ch-2 and Ch-10 eigenvalues. Right) Ch-2and Ch-10 Spectrograms.

5.5.1 Fast Fading Ch-2 BER Vs. SNR

Average receiver Speed	20 km/h
Distance of evaluation interval N_F	2.93 m
Distance of estimation interval N_P	56.3 m

Table 5.5 Channel 2 speed and distance information

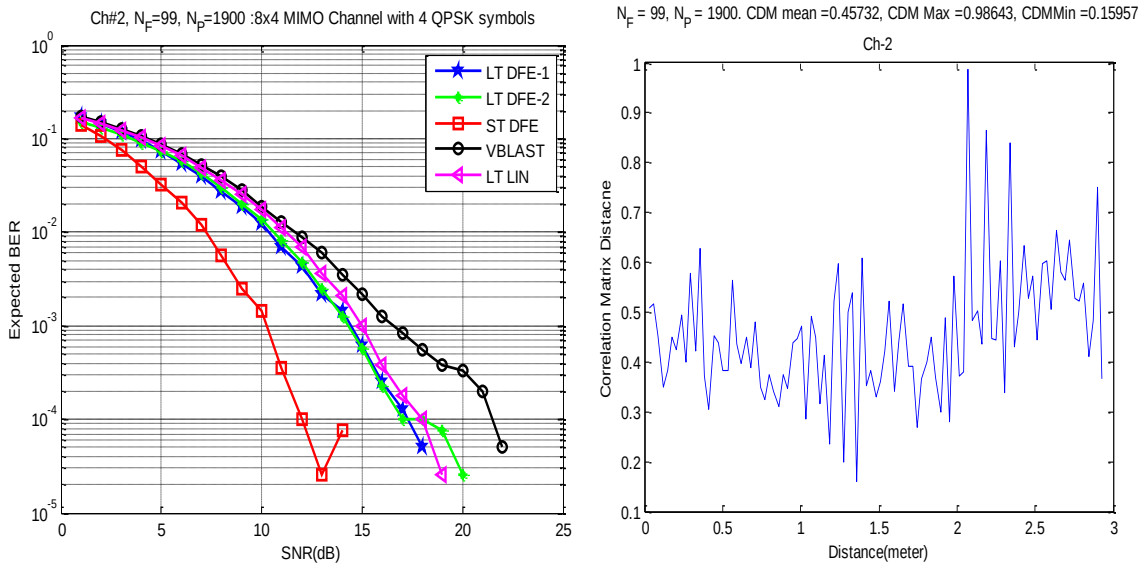

Figure 5.9: (Left) Performance of precoder designs over Ch-2 in terms of BER. (Right) CMD of Expected $\boldsymbol{R}_{Tx}$ of estimation interval with $\boldsymbol{R}_{Tx}$'s **o**f evaluation interval.

Figure 5.9. (left) shows the performance of the considered precoder designs on the fast channel. It is clear from Figure 5.9. (left) that the long-term precoders with DFE receivers (LT DFE-1 and LT DFE-2) have almost no difference in their performance and they outperform the long-term precoder with linear receiver (LT LIN) because of the advantage of DFE. The performance curves of the long term precoders are located in the middle of the performance curves of optimal precoder and VBLAST and closer to the VBLAST.

5.5.2 Fast Fading Ch-10 BER Vs. SNR

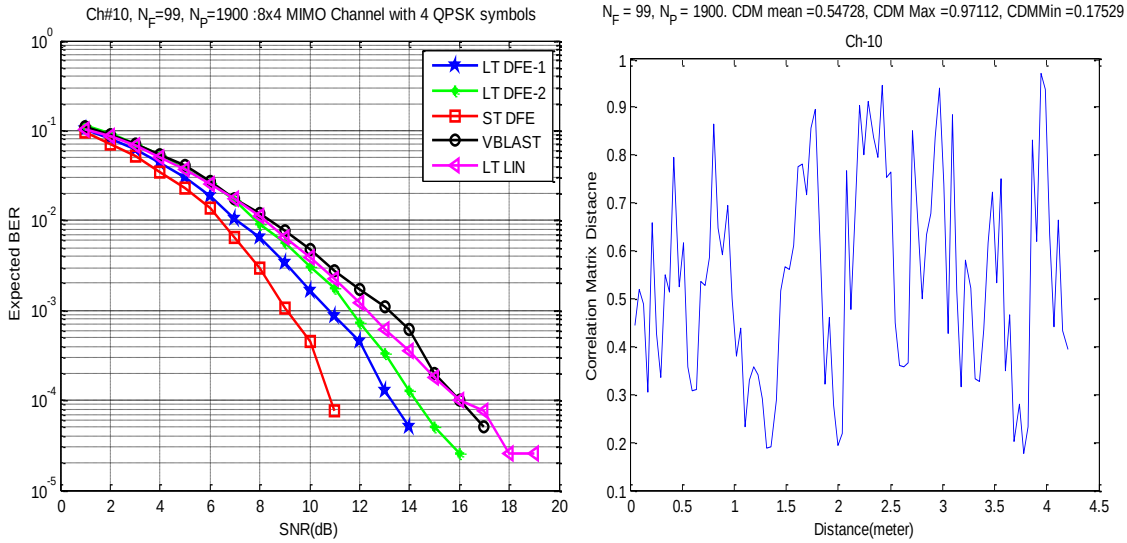

Figure 5.10: (Left) Performance of precoder designs over Ch-10 in terms of BER. (Right) CMD of Expected $\boldsymbol{R}_{Tx}$ of estimation interval with $\boldsymbol{R}_{Tx}$'s **o**f evaluation interval

Average receiver Speed	29 km/h
Distance of evaluation interval N_F	4.2 m
Distance of estimation interval N_P	81.71 m

Table 5.6 Channel 10 speed and distance information

It is clear from Figure 5.10. (left) the LT DFE-1 precoder outperforms the other long-term precoders and the VBLAST. LT DFE-1 performance curve approaches the performance of the optimal precoder (ST DFE). Figure 5.10. (right) shows the high dynamic range in CMD.

5.6 Fast-Fading Channel Ch-12 and Ch-14

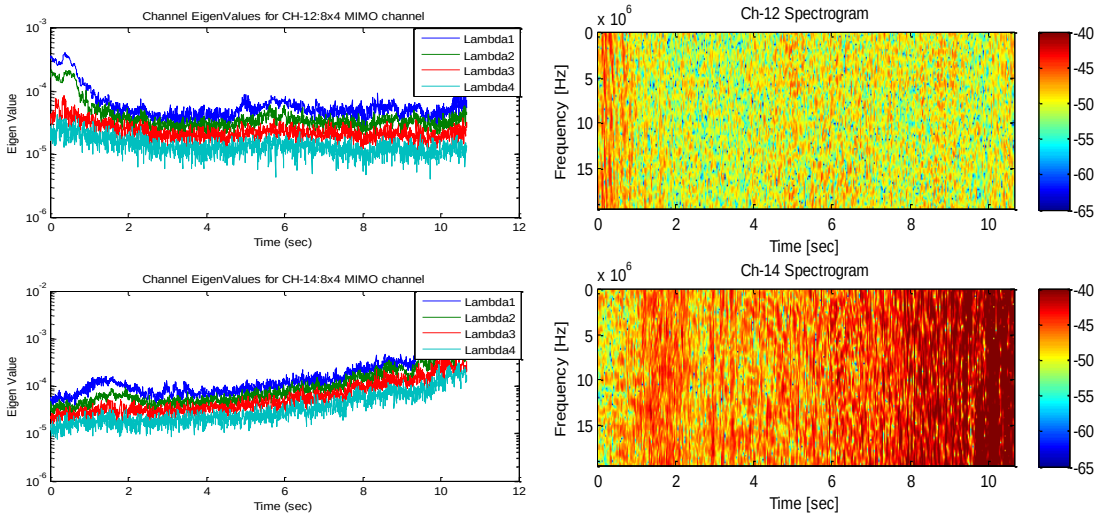

Figure 5.11: Left) Ch-12and Ch-14 eigenvalues. Right) Ch-12and Ch-14 Spectrograms.

5.6.1 Fast Fading Ch-12 BER Vs. SNR

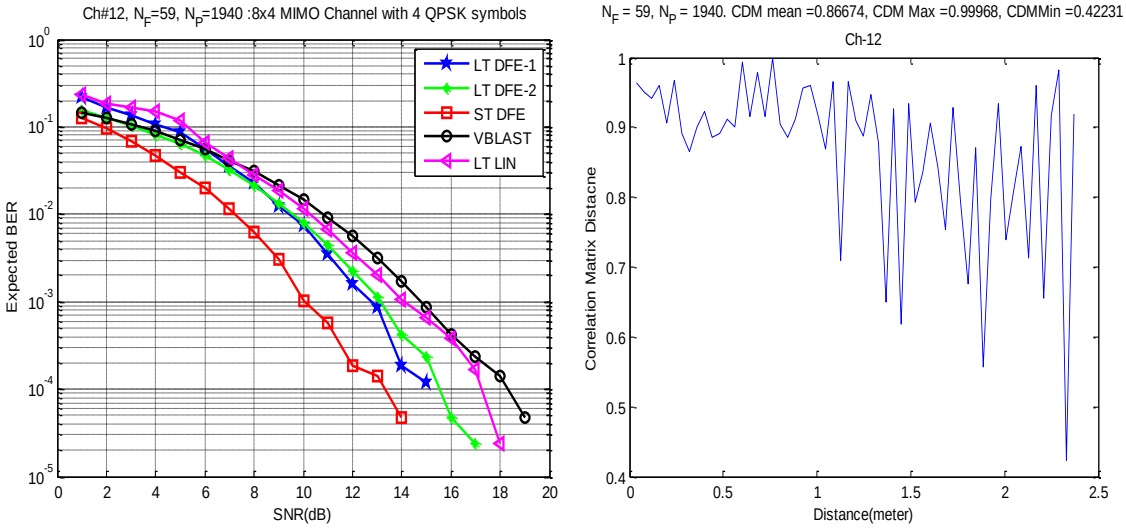

Figure 5.12: (Left) Performance of precoder designs over Ch-12 in terms of BER. (Right) CMD of Expected $\boldsymbol{R}_{Tx}$ of estimation interval with $\boldsymbol{R}_{Tx}$'s **o**f evaluation interval.

Average receiver Speed	27.1 km/h
Distance of evaluation interval N_F	2.37 m
Distance of estimation interval N_P	77.9 m

Table 5.7 Channel 12 speed and distance information

In Figure 5.12. (left) the long-term precoders with DFE receivers (LT DFE-1 and LT DFE-2) almost have the same performance and work better than the long-term precoder with linear receivers (LT LIN) and VBLST. Figure 5.12. (right) shows the high dynamic range in CMD.

5.6.2 Fast Fading Ch-14 BER Vs. SNR

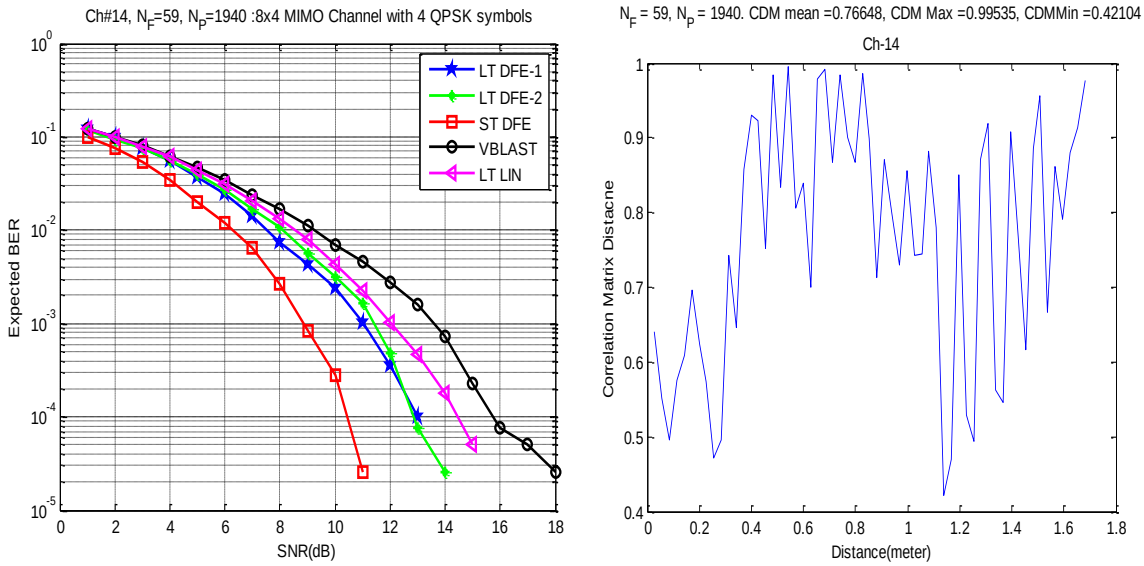

Figure 5.13: (Left) Performance of precoder designs over Ch-14 in terms of BER. (Right) CMD of Expected $\boldsymbol{R}_{Tx}$ of estimation interval with $\boldsymbol{R}_{Tx}$'s **o**f evaluation interval

We note the same conclusions of the previous section.

Average receiver Speed	19.2 km/h
Distance of evaluation interval N_F	1.68 m
Distance of estimation interval N_P	55.15 m

Table 5.8 Channel 14 speed and distance information

5.7 Fast-Fading Channel Ch-22 and Ch-27

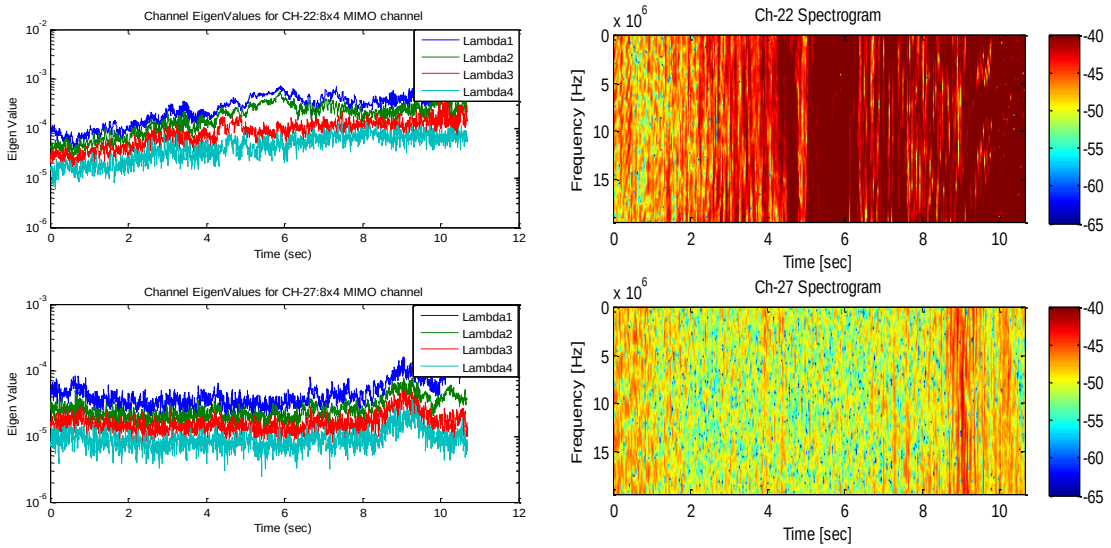

Figure 5.14: Left) Ch-22 and Ch-27 eigenvalues. Right) Ch-22and Ch-27 Spectrograms.

5.7.1 Fast Fading Ch-22 BER Vs. SNR

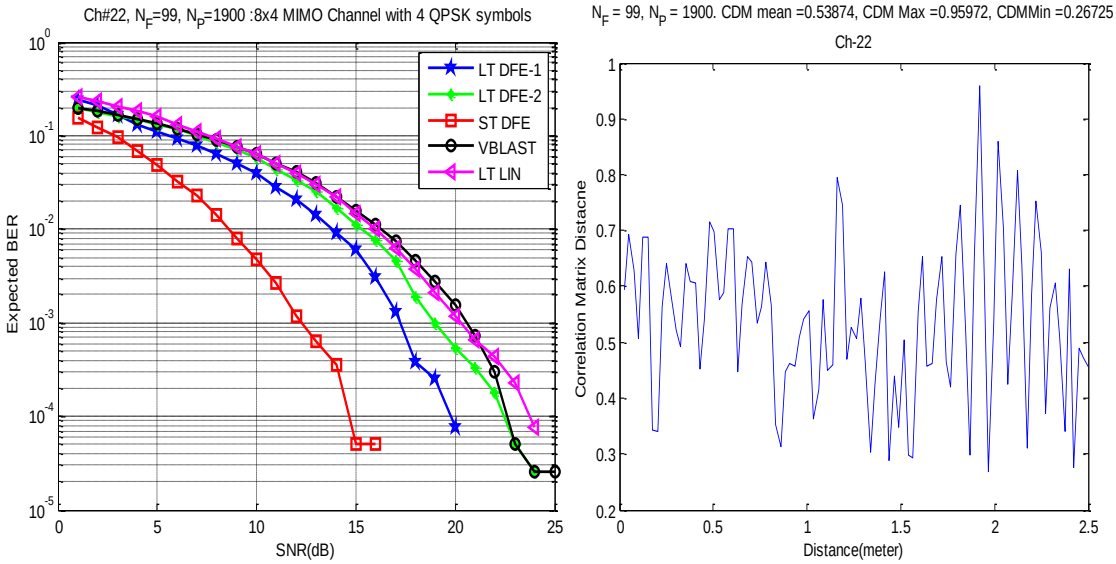

Figure 5.15: (Left) Performance of precoder designs over Ch-22 in terms of BER. (Right) CMD of Expected $\boldsymbol{R}_{Tx}$ of estimation interval with $\boldsymbol{R}_{Tx}$'s of evaluation interval

Here, it is clear the LT DFE-1 outperforms other long term precoders (LT DFT-2 and LT LIN) and VBLST. The optimal precoder ST DFE significantly outperforms all others precoders.

Average receiver Speed	17.2 km/h
Distance of evaluation interval N_F	2.5 m
Distance of estimation interval N_P	48.2 m

Table 5.9 Channel 22 speed and distance information

5.7.2 Fast Fading Ch-27 BER Vs. SNR

Average receiver Speed	27.2 km/h
Distance of evaluation interval N_F	4.0 m
Distance of estimation interval N_P	76.6 m

Table 5.10 Channel 27 speed and distance information

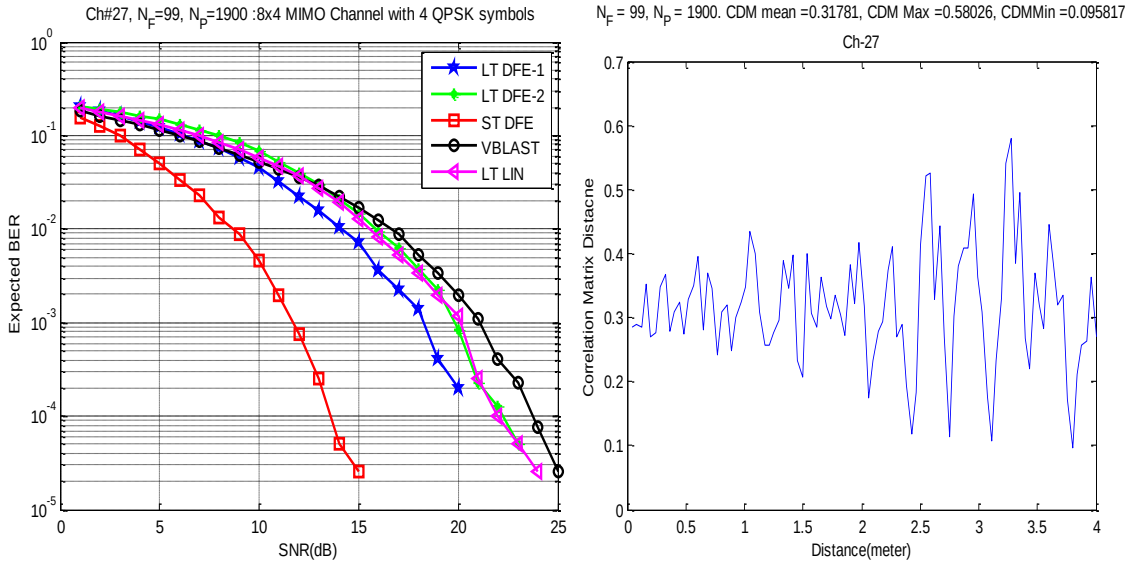

Figure 5.16 Left) Performance of precoder designs over Ch-27 in terms of BER. Right) CMD of Expected $\boldsymbol{R}_{Tx}$ of estimation interval with $\boldsymbol{R}_{Tx}$'s **o**f evaluation interval

We note the same conclusions of the previous section.

Part III

Conclusion

6 Conclusion and Future work

6.1 Conclusion

We have evaluated the performance of five different precoder designs on 8x4 MIMO channel measurements. Our main focus was on the performances of long-term precoder designs, for their similarity to the scenarios in the real situations of CSI at wireless communication systems. The precoder designs have been evaluated over different channel characteristic types, (i) Slow Fading Channel, (ii) Fast Fading Channel, and (iii) Line of Sight Channel. The recent proposed long-term precoder in [1] has demonstrated better performance compared to other long-term designs which are considered in this evaluation [3, 4]. To have almost complete background about the characteristics of the channel portions that were used in this evaluation, the spectrograms and the eigenvalues that vary with time are plotted and added next to the plots of the performance evaluations. Since the long-term precoders rely on statistical information of the channel matrix, the correlation matrix distance (CMD) between the estimated correlation transmit matrix (estimated of the estimation interval) and the correlation transmit matrices of the channel matrix samples in the evaluation interval are computed.

6.2 Future Work

Study the spatial correlation of the measured channel, and find the relationship between the long-term precoders performance and the amount of spatial correlation of the channel.

References:

[1] S. Järmyr, S. Bergman, G. Ottersten, "Long-term adaptive precoding for decision feedback equalization," IEEE international conference, pp.2897-2900, 2008.

[2] D.P. Palomar and Y. Jiang, MIMO Tranceiver Design via Majorization Theory, Now Publishers Inc., 2007.

[3] O. Simeone, Y. Bar-Ness, and U. Spagnolini, "Linear and nonlinear preequalization/equalization for MIMO systems with long-term channel state information at the transmitter," IEEE Transactions on Wireless Communications, vol. 3, pp. 373–378, 2004.

[4] X. Zhang, D.P. Palomar, and B. Ottersten, "Statistically robust design of linear MIMO transceivers," IEEE Transactions on Signal Processing, vol.56, pp. 3678-3689, 2008.

[5] P.W.Wolniansky, G.J. Foschini, G.D. Golden, and R.A. Valenzuela, "V-blast: An architecture for realizing very high data rates over the rich-scattering wireless channel," URSI International Symposium on Signals, Systems, and Electronics, pp. 295–300, 1998.

[6] K. Yu, M. Bengtsson, B. Ottersten, P. Karlsson, and M. Beach, "Second order statistics of NLOS indoor MIMO channels based on 5.2 GHz measurements," in Proceedings of IEEE Global Telecommunications Conference, vol. 1, pp. 156–160, Dec. 2001.

[7] D. Chizhik, J. Ling, P. W. Wolniansky, R. A. Valenzuela, N. Costa, and K. Huber, "Multiple-input-multiple-output measurements and modeling in Manhattan," IEEE J. Sel. Areas Commun., vol. 21, pp. 321–331, Apr. 2003.

[8] M. Herdin and E. Bonek, "A MIMO Correlation Matrix based Metric for Characterizing Non- Stationarity", in the IST Mobile and Wireless Communications Summit, Lyon, 2004.

[9] G. H. Golub and C. F. V. Loan, Matrix Computation. Baltimore, MD: The Johns Hopkins University Press, thired ed., 1996.

[10] Hassibi, "A fast square-root implementation for BLAST," Thirty-Fourth Asilomar Conference on Signals, Systems and Computers, pp. 1255–1259, November 2000.

[11] D. P. Palomar, J. M. Cioffi, and M. A. Lagunas, "Joint Tx-Rx beamforming design for multicarrier MIMO channels: a unified framework for convex optimization," IEEE Transactions on Signal Processing, vol. 51, no. 9, pp. 2381-2401, Sept. 2003.

[12] Yi Jiang, William W. Hager, Jian Li, "THE GENERALIZED TRIANGULAR DECOMPOSITION", mathematic of computation, vol. 77, no.262, pp. 1037-1056, April 2008.